



**HAL**  
open science

## Modeling of ray paths of head waves on irregular interfaces in TOFD inspection for NDE

Adrien Ferrand, Michel Darmon, Sylvain Chatillon, Marc Deschamps

► **To cite this version:**

Adrien Ferrand, Michel Darmon, Sylvain Chatillon, Marc Deschamps. Modeling of ray paths of head waves on irregular interfaces in TOFD inspection for NDE. *Ultrasonics*, 2014, 54 (7), pp.1851 - 1860. 10.1016/j.ultras.2013.12.007 . hal-01836190

**HAL Id: hal-01836190**

**<https://hal.science/hal-01836190>**

Submitted on 3 Jan 2019

**HAL** is a multi-disciplinary open access archive for the deposit and dissemination of scientific research documents, whether they are published or not. The documents may come from teaching and research institutions in France or abroad, or from public or private research centers.

L'archive ouverte pluridisciplinaire **HAL**, est destinée au dépôt et à la diffusion de documents scientifiques de niveau recherche, publiés ou non, émanant des établissements d'enseignement et de recherche français ou étrangers, des laboratoires publics ou privés.

## Accepted Manuscript

Modeling of ray paths of head waves on irregular interfaces in TOFD inspection for NDE

A. Ferrand, M. Darmon, S. Chatillon, M. Deschamps

PII: S0041-624X(13)00345-4

DOI: <http://dx.doi.org/10.1016/j.ultras.2013.12.007>

Reference: ULTRAS 4733

To appear in: *Ultrasonics*



Please cite this article as: A. Ferrand, M. Darmon, S. Chatillon, M. Deschamps, Modeling of ray paths of head waves on irregular interfaces in TOFD inspection for NDE, *Ultrasonics* (2013), doi: <http://dx.doi.org/10.1016/j.ultras.2013.12.007>

This is a PDF file of an unedited manuscript that has been accepted for publication. As a service to our customers we are providing this early version of the manuscript. The manuscript will undergo copyediting, typesetting, and review of the resulting proof before it is published in its final form. Please note that during the production process errors may be discovered which could affect the content, and all legal disclaimers that apply to the journal pertain.

1 **Modeling of ray paths of head waves on irregular interfaces in TOFD inspection for**

2 **NDE**

3 **A. Ferrand<sup>1</sup>, M. Darmon<sup>1</sup>, S. Chatillon<sup>1</sup> and M. Deschamps<sup>2</sup>**

4 <sup>1</sup>CEA, LIST, Department of Imaging & Simulation for Nondestructive Testing, F-91191 Gif-  
5 sur-Yvette, France.

6 <sup>2</sup> Univ. Bordeaux, I2M-APy, UMR 5295, 33400 Talence, France.

7

8 **E-mail authors:**

9 A. Ferrand: adrien.ferrand@cea.fr

10 M. Darmon: michel.darmon@cea.fr

11 S. Chatillon: sylvain.chatillon@cea.fr

12 M. Deschamps: m.deschamps@i2m.u-bordeaux1.fr

13

14 **Corresponding author:**

15 M. Darmon

16 Phone number: (+33)169082288

17 Email: michel.darmon@cea.fr

18 Postal address: CEA, LIST, Department of Imaging & Simulation for Nondestructive Testing,

19 F-91191 Gif-sur-Yvette, France.

20

21 **Abstract:**

22 The TOFD (Time Of Flight Diffraction) technique is a classical ultrasonic inspection method  
23 used in ultrasonic non-destructive evaluation (NDE). This inspection technique is based on an  
24 arrangement of two probes of opposite beam directions and allows a precise positioning and a  
25 quantitative evaluation of the size of cracks contained in the inspected material thanks to their  
26 edges diffraction echoes. Among the typical phenomena arising for such an arrangement,  
27 head waves, which propagate along the specimen surface and are chronologically the first  
28 waves reaching the receiver, are notably observed. Head wave propagation on planar surfaces  
29 in TOFD configurations is well known. However, realistic inspection configurations often  
30 involve components with irregular surfaces, like steel excavated specimens.

31 Surface irregularity is responsible for numerous effects on the scattering of bulk waves,  
32 causing the melting of surface and bulk mechanisms in the head wave propagation. In order to  
33 extend the classical ray approach on these complex cases, a generic algorithm of ray tracing  
34 between interface points (GIRT) has been designed. With respect to time of flight  
35 minimization (i.e. the generalized Fermat's principle), ray paths can be computed by GIRT  
36 for different natures of waves scattered by the complex surfaces or by flaws. The head wave  
37 fronts computed by GIRT are notably in good agreement with FEM simulated results. This  
38 algorithm, based on pure kinematic analysis of waves propagation, represents a first step in  
39 the future development of a complete ray theory for head waves simulation on irregular  
40 interfaces.

41

42 **Keywords:**

43 head wave, ray tracing algorithm, irregular surface, wave diffraction, non-destructive  
44 evaluation

45

46 **1. Introduction**

47

48 Head waves are well known phenomena occurring in seismic inspections: they correspond  
49 to the first wave received by seismic probes, giving so their names. Typical seismic  
50 inspections deal with configurations involving two media separated by a planar interface.  
51 Specific wave theories have been developed, all considering head waves on planar surfaces as  
52 critically refracted waves. These modeling approaches are based on an asymptotic integral  
53 evaluation [1], the asymptotic ray theory [2,3] or the generalized ray theory (Cagniard-De  
54 Hoop method) [4,5]. It is shown that the head wave on planar interfaces corresponds to the  
55 combination of both waves travelling along one interface side with the corresponding material  
56 sound velocity (compulsory more than that of the incident wave), and bulk waves radiated  
57 from the interface towards one material and propagating at the critical angle. The waves  
58 propagating along the interface are composed of the well-known lateral waves [1–6] and of  
59 the Goodier-Bishop type waves [7] for the case of a finite beam impacting the interface.

60 Head waves on planar surfaces are also observed in NDE by using specific techniques and  
61 similar configurations than the seismic ones. Among the various NDE inspections techniques,  
62 the Time of Flight Diffraction (TOFD) technique allows a precise and quantitative evaluation  
63 of surface breaking or embedded cracks. This technique uses two probes moving on the  
64 inspected material surface with a fixed Probe Center Spacing (PCS). The TOFD configuration  
65 is particularly well adapted to generate and receive head wave signals [8–10] (sometimes used  
66 for surface breaking cracks detection).

67 The CIVA software platform for NDE simulation, developed at CEA/LIST, enables a  
68 complete simulation of TOFD inspections: indeed different semi-analytical models [8,11,12]  
69 have been integrated to model all the echoes observed in a TOFD configuration (head wave,

70 flaw edges diffractions, back wall echo...). The developed model for head waves simulation  
71 is based on the asymptotic ray theory [3] which has also been used to improve the modeling  
72 of flaw corner echoes [13,14]. Nevertheless, the existing head wave simulation can only be  
73 applied for a planar specimen composed of an isotropic medium.

74 TOFD and other pitch-catch configurations are also classically used on non-planar  
75 interfaces both in NDE (inspections of cylinders, nozzles [8].) and in the seismic domain:  
76 indeed in works carried out by Zhou and Chen [15], head wave travel times have been  
77 calculated by numerical simulations on some irregular surfaces for some seismic inspections.  
78 It has been shown that the head wave propagation is more complex on irregular surfaces than  
79 on planar surfaces. Indeed, whereas the head wave on a planar interface is due to the critical  
80 refraction of the incident wave and includes a surface wave component propagating along the  
81 planar surface (called lateral wave), the head wave propagation on irregular surfaces implies  
82 propagations in the material bulk. The received head wave signal on irregular surfaces has a  
83 different amplitude than in the planar case and a travel time compatible with the hypothesis of  
84 propagation in the material bulk. Analytical modelings of the head wave propagation around  
85 the Earth have also been proposed in several seismic studies. Indeed, using an integral  
86 representation of the solution, the received head wave signal has been evaluated for slightly  
87 curved irregularities [16,17] of surface parametric equation  $F(x) = x^2 / 2D$  with large values of  
88 the radius of curvature  $D$  compared to the surface size, and for spherically symmetric radially  
89 heterogeneous media [18]. These studies confirms conclusions given in [15] concerning the  
90 time of flight and the amplitude of the head wave.

91 In the present study, complete interpretation and simulation of the head wave propagation  
92 mechanisms for irregular surfaces are proposed. This approach leads to the development of a  
93 generic algorithm of ray tracing between interface points (called in the following for  
94 simplification Generic Interface Ray Tracing/GIRT) which is able to compute the travelling

95 path of head waves in specimens inspected by TOFD technique. Based on an adaptation to the  
96 NDE domain of seismic ray tracing algorithms, GIRT is a new method for solving the two-  
97 points ray tracing problem, which is the calculation of the true ray between two defined  
98 points: the source and observation points.

99 Ray-tracing techniques are often employed for modeling wave propagation in  
100 electromagnetism, optics, seismology ... Traditional ray tracing algorithms are the shooting  
101 method [19] and the bending method [20,21]. The shooting method, well adapted for field  
102 propagation modeling, fixes the source point, takes initial ray direction and then finds the  
103 location of the observation point; in the view of two-points rays tracing, an iterative procedure  
104 for finding the starting direction can be used to yield the desired observation point. Ray  
105 bending is a variational approach which perturbs some initial estimate of the ray path, the  
106 ends being fixed, until the true ray which minimizes the travel time is found. The two  
107 previous traditional methods are heavy in time computation for solving the two-points ray  
108 tracing problem and not efficiently adapted to deal with diffracted waves and shadow areas in  
109 which head waves around irregular surfaces propagate.

110 To improve efficiency of the shooting method on the diffracted waves calculation, seismic  
111 ray tracing algorithms based on a grid based scheme were developed more recently : wave  
112 front construction [22], the finite difference Eikonal equation solver [23–27] which also

113 generally needs large computation time for tracing rays and Shortest Path Method (SPM)  
114 algorithms [28–35] (also called minimum travel time tree - MTTT) which are relatively  
115 underdeveloped algorithms based on Huygens' and Fermat's principles. Compared with the  
116 traditional ray tracing algorithms, the grid based scheme has several advantages for

117 application to NDE modeling: it is able to easily locate ray paths in shadow zones; it is  
118 numerically stable and can find the first arrival in complex media.

119 The current study proposes, for modeling the propagation of an incident beam towards a  
120 receiving probe in a specimen of irregular surfaces including flaws, an approach based on  
121 seismic SPM algorithms adapted to ultrasonic NDE and specifically designed for the two  
122 points ray tracing problem. For a 2D propagation, the initial SPM Moser's algorithm [29]  
123 consists in launching rays from a source, in considering in a 2D grid the adjacent node with  
124 minimal travel time as a secondary source, in repeating the previous process so as to  
125 propagate first arrival waves to the 2D grid nodes. More recently, Zhang et al [35] developed  
126 the interface source method (ISM): as in Moser's SPM, first arrival waves still propagate  
127 using a ray shooting scheme from nodes to nodes in a 2D grid but on the other hand only  
128 interface points are taken as secondary sources. The developed GIRT model uses a new SPM  
129 approach specifically devoted to two points ray tracing in a propagation medium constituted  
130 of homogeneous volumes (in terms of sound velocity). The GIRT takes advantages that in the  
131 latter case waves propagate in straight lines between interface points: only the specimen  
132 interfaces are meshed (in a simple 1D mesh for a 2D propagation), the source (on the emitter)  
133 and observation (on the receiver) points are added to the mesh and the wave ray path of  
134 minimum travel time passing through mesh points is found between the two fixed points. One  
135 of the major advantages of this GIRT method is the fast processing of very irregular surfaces  
136 as only the surfaces of the specimen are meshed and not all the specimen volume like in other  
137 SPM algorithms [28–35]. In addition, GIRT directly traces in an optimized manner (a two  
138 points ray tracing) the shortest path from a source reaching any required observation point  
139 located anywhere (outside the 2D grids needed by previous methods to propagate all shortest  
140 paths to all grid nodes).

141 Furthermore, compared to the ISM method [35], the developed GIRT algorithm has  
142 notably added features to meet the specificities of ultrasonic NDT applications. Firstly,  
143 whereas ISM has been shown to deal with only the first arrival or one reflection path for P  
144 bulk waves, the GIRT algorithm is adapted to find not only the head wave ray path (first  
145 arrival) but also all complex later arrival waves including mode or nature conversion by  
146 adding constraints on the searched ray path, fixing one or more points through which the ray  
147 path must pass, and by defining independent types of wave propagation along each path  
148 connecting the constraint points. Secondly, the GIRT can take into account all types and  
149 natures of waves propagation occurring in NDE. Indeed the propagation is available not only  
150 for the SH head waves studied in [15] (also called TH) but also for P and SV waves (also  
151 called L and TV). Surface waves as Rayleigh waves and head waves are taken into account as  
152 well as diffractions from surfaces in any kind of waves. Finally, GIRT approach is extended  
153 to flaw scattering modeling since the flaws contained in the specimen are also meshed by the  
154 GIRT algorithm in order to model rays diffracted from flaws. Consequently the GIRT  
155 algorithm is generic for application to NDE as it can deal with any ultrasonic wave  
156 propagating near irregular surfaces or flaws of any geometry (CAD defined). Finally this tool  
157 is able to calculate valid geometric ray paths after interaction with interfaces or flaws. One  
158 interest of the study presented in this paper is also to evaluate the applicability of such a  
159 method initially based on seismic ray tracing in NDE applications for which the characteristic  
160 dimensions (propagation distance or scatterer size) to the wave length ratio can be smaller than in  
161 geophysics. The current study shows that GIRT leads to a better understanding of the head  
162 wave propagation and its interaction with the surfaces. In that aim, a data fusion of simulated  
163 results obtained by both GIRT and a FEM-based method is carried out.

164 The paper is organized as follows. The theoretical principles of the approach, the GIRT  
165 algorithm process and the GIRT capabilities are described in section 2; some ray tracings and

166 wave fronts of the head wave and some later arrival waves, simulated with GIRT in 2D  
167 applications, are compared for validation with FEM results in section 3.

168

## 169 **2. The Generic Interface Ray Tracing (GIRT) method**

170

171 The development of a ray tracing method allows a better understanding of the head wave  
172 propagation on irregular surfaces by providing valid ray paths. The interest of such a study is  
173 described in parts 2.1 and 2.2. The developed ray tracing method (GIRT) is generic by the fact  
174 that it supports any kind of wave propagation and interaction with an irregular surface, and  
175 describes the physical phenomena involved in the head wave propagation. Its theoretical  
176 principles, functionalities and operating process are detailed in part 2.3.

177

### 178 **2.1. Head waves in planar surfaces configurations**

179

180 For a planar surface inspected in TOFD, a head wave is generated at the interface between  
181 the material and the emitter and propagates in the material along the surface, and is radiated as  
182 a bulk wave in the wedge, reaching the receiver. For planar surfaces, the head wave is seen as  
183 the result of a critical refraction phenomenon of the incident wave on the interface between  
184 the two media. *Fig. 1* describes, in a TOFD inspection of a planar specimen containing an  
185 embedded crack, the propagation of different waves including the head wave.

186 *Fig. 2* illustrates the B-scan measured in the inspection described in *Fig. 1*. Three kinds of  
187 signals can be observed and are characteristics of a TOFD inspection on a planar specimen.

188 These signals correspond respectively to the head wave (1), the diffraction (2, 2') of the  
189 refracted bulk wave on the edges of the crack and the reflection (4) of the refracted bulk wave  
190 on the specimen bottom.

191

192 **2.2. Head wave in irregular surfaces configurations**

193

194 TOFD inspections of specimen with irregular entry surfaces can be required for specific  
195 NDE applications. For example, the process of repairing a material including a surface  
196 breaking crack implies to remove the matter around the defect then to replace the removed  
197 matter. The TOFD technique is applied on the specimen between the two reparation stages in  
198 order to ensure that the entire defect has been removed. The geometry of the specimen after  
199 matter removing is presented in *Fig. 3*.

200 A good understanding of the head wave propagation on such surfaces is essential for the  
201 complete modeling of TOFD inspections on realistic configurations. In particular, the head  
202 wave signal is one of the main references for the detection and the location of potential  
203 defects in the specimen. As explained in [15], irregularities of the specimen surface induce  
204 modifications on the head wave received signal compared to that observed on planar  
205 interfaces. Indeed such modifications can be noticed on experiments: the B-scan presented in  
206 *Fig. 4* is extracted from a TOFD inspection measurement on the specimen described in *Fig. 3*  
207 and highlights two kinds of differences which can be observed when scanning over the  
208 surface irregularities. Firstly, the head wave time of flight appears to be incoherent with the  
209 hypothesis of head wave propagation all along the entry surface: indeed the measured travel  
210 time is less than that of a surface wave propagating all along the complex surface. Secondly,  
211 the irregular surface causes an important decrease (more than 15dB) of the head wave  
212 amplitude compared to a planar interface.

213 To understand the physical process responsible for the observed head wave propagation on  
214 complex surfaces, an analysis of the nature of the field propagating near such surfaces has  
215 been carried out: the emitter generates a refracted field in the material which interacts with the

216 surface. In particular, surface corners are responsible for diffracting the field in their  
217 geometrical shadow. Thus head wave propagation cannot be considered as a critical refraction  
218 anymore like in the case of planar surfaces, but the result of the diffractions of the generated  
219 refracted field on the surface irregularities. *Fig 5a* describes such behavior on an example of  
220 irregular surface: the head wave, after a bulk refraction of the incident wave, is diffracted two  
221 times on the surface corners, in order to create a diffracted wave, which is then refracted again  
222 towards the receiver. In order to visualize this behavior, some numerical simulations have  
223 been carried out with the hybrid technique CIVA/ATHENA [36] using both analytical models  
224 and finite elements simulations near the surface irregularities. The principle of this technique  
225 is the following. A volume in the specimen is defined, embedding the surface and its  
226 irregularities. The field reaching the volume entry is calculated by the analytical CIVA pencil  
227 method on the volume border. Then the field is propagated in the defined volume by the finite  
228 elements scheme ATHENA. The results of this simulation are presented in *Fig. 5b* and show  
229 that there exists a field diffracted from the surface corner in the geometrical shadow area of  
230 the irregular surface: the corresponding diffracted rays will generate the head wave (*Fig 5a*).

231

### 232 **2.3. GIRT objectives and principles: construction of valid ray paths**

233

234 Considering the behavior of the head wave near an irregular surface, the ray theory  
235 formalism is then applied for the two points ray tracing problem. The head wave propagation  
236 and more generally all the waves in the specimen are then the result of specific interactions  
237 between the wave field inside or outside the specimen and the specimen surface: the ray path  
238 representing this propagation is the combination of specific rays connected to each other by  
239 secondary source points. These secondary source points are located on the specimen surface

240 and correspond to the locus of each interaction responsible of the wave propagation. The rays  
 241 are a representation of the wave propagation between each secondary source points.

242 The GIRT ray tracing formalism is thus based on the Huygens principle. Considering  
 243 known source point  $M_s$  and observation point  $M_o$ , there exists a secondary source points  
 244 collection  $\{M_i\}_{i \in (1, \dots, N)}$  located on the specimen/flaws surfaces which represents the locus of all  
 245 potential interactions between the wave field and the surfaces: the size  $N$  of the secondary  
 246 source points increases with the complexity of the surface irregularities. The ray path  
 247 associated to a wave propagation between the points  $M_s$  and  $M_o$  is then a combination of  
 248 elementary particular rays  $(M_j M_l)_{(j,l) \in (s,o,1, \dots, N)^2}$  whose extremities are secondary source points  
 249  $M_i$  among the collection  $\{M_i\}_{i \in (1, \dots, N)}$  of an elementary ray emitted from  $M_s$  and of an  
 250 elementary received on  $M_o$ .

251 In the following, it is illustrated on examples (*Fig. 6*) that this principle of secondary  
 252 sources can be applied to represent all physical waves in a propagation medium containing  
 253 interfaces and flaws. In a general manner, numerous waves including the head wave are  
 254 emitted from a source point  $M_s$  and received on an observation point  $M_o$ : these waves are  
 255 characterized by their interactions with the specimen surfaces involved in their propagation  
 256 and then by the secondary source points constructing the associated ray path. Moreover,  
 257 these interactions may be responsible of a wave mode or wave nature conversion:  
 258 consequently, each elementary ray  $(M_j M_l)_{(j,l) \in (s,o,1, \dots, N)^2}$  can represent the propagation of a  
 259 longitudinal (L) bulk wave, transversal bulk waves (T in an isotropic medium, qT1 and qT2 in  
 260 anisotropic one), lateral surface wave (L or T) or Rayleigh-like (Rayleigh, Generalized  
 261 Rayleigh, Stoneley) wave depending on the type of interaction located on the secondary  
 262 source point  $M_j$  which is the departure point of ray  $(M_j M_l)_{(j,l) \in (s,o,1, \dots, N)^2}$ .

263 Two inspection configurations involving irregular surfaces are studied as examples in *Fig.*  
 264 6. The first configuration (*Fig. 6a*) is a three propagation media one for inspection of a  
 265 specimen including a corner irregularity on its entry surface, an internal interface with slopes  
 266 and a defect. The case of an isotropic elastic specimen with an entry cylindrical surface is  
 267 shown in *Fig. 6b*. The upper medium is a fluid one in both cases. Each ray path in *Fig. 6a* and  
 268 *Fig. 6b* represents one particular wave propagating. Only some ray paths among all existing  
 269 are shown as examples and the secondary source collection  $\{M_i\}_{i \in \{1, \dots, N\}}$  is consequently not  
 270 exhaustive.

271 As to the configuration of *Fig. 6a*, the ray path  $M_s M_2 M_5 M_{12} M_o$  (path 1) is the ray with the  
 272 shortest time of flight and thus corresponds to the head wave propagation: its path is  
 273 composed of a refraction at  $M_2$  of the longitudinal bulk wave emitted at  $M_s$ , a corner  
 274 diffraction at  $M_4$  without mode or nature conversion and a refraction towards the observation  
 275 point  $M_o$ . However the diffraction of the L bulk wave at the corner  $M_5$  implies also a mode  
 276 conversion into a T wave and gives after refraction at  $M_{11}$  the ray path  $M_s M_2 M_5 M_{11} M_o$  (path  
 277 2 in *Fig. 6a*) with a higher time of flight than the head wave ray path. The ray path  
 278  $M_s M_3 M_4 M_5 M_7 M_{10} M_o$  (path 3) is associated to a L bulk wave critically refracted at  $M_3$  into a  
 279 L lateral wave which propagates along the surface and is critically reradiated at  $M_{10}$  into a  
 280 bulk L wave. As another example the secondary source point  $M_7$  also converts the lateral  
 281 wave into a Rayleigh wave which radiates at  $M_9$  a bulk L wave and gives the ray path  
 282  $M_s M_3 M_4 M_5 M_7 M_9 M_o$  (path 4). Finally the ray path  $M_s M_1 M_6 M_8 M_{13} M_o$  (path 5) corresponds  
 283 to a L bulk wave emitted at  $M_s$  and refracted at  $M_1$  which is reflected on the internal  
 284 interface of the specimen on  $M_6$  and diffracted on the edge defect on  $M_8$  before reaching  
 285  $M_o$ .

286 *Fig. 6b* shows the ray paths of different waves which propagate close to a surface with a  
 287 cylindrical irregularity. The head wave propagation is associated to the shortest ray path  
 288  $M_s M_1 M_4 M_5 M_9 M_o$  (path 1): the emitted L bulk wave is refracted in the specimen at  $M_1$  and  
 289 diffracted on the cylindrical irregularity in a surface creeping ray  $M_4 M_5$ ; the wave propagates  
 290 along the irregularity and is then radiated again at  $M_5$ , and refracted at  $M_9$  towards the  
 291 observation point  $M_o$ . Similarly to the path 3 of *Fig. 6a* along the corner irregularity, the ray  
 292 path 2 ( $M_s M_2 M_3 M_6 M_8 M_o$ ) represents the L lateral wave propagation along the cylindrical  
 293 irregularity generated by a critical refraction at  $M_2$  and the critical radiation at  $M_8$ . A  
 294 Rayleigh wave is also created at  $M_6$  which radiates at  $M_7$  and give the path 3  
 295  $M_s M_2 M_3 M_6 M_7 M_o$ .

296 Ray paths not shown on *Fig. 6a* and *Fig. 6b* result from other interactions in the specimen.  
 297 For example, mode conversion of the emitted L bulk wave occurs at the refraction on the  
 298 entry surface, at specular reflections or at diffractions on the specimen surface irregularities or  
 299 flaws (like at  $M_8$  in *Fig. 6a*) and allows the propagation of several transversal bulk waves  
 300 into the specimens. Mode conversions of bulk waves into Rayleigh-like waves also occurs on  
 301 surface irregularities (at  $M_4$ ,  $M_5$ , ... in *Fig. 6a* or  $M_3$  in *Fig. 6b*).

302 Finally the purpose of the GIRT is to find all physical paths described above in isotropic or  
 303 anisotropic media using the Generalized Fermat's Principle. This principle is a basic one of an  
 304 asymptotic ray theory, the Geometrical Theory of Diffraction (GTD) [37] which extends  
 305 Geometrical Acoustics by adding rays diffracted from canonical scatterers (edges, corners,  
 306 curved smooth objects...) to the classical geometrical (refracted and reflected) rays. In the  
 307 aim of ray tracing, the Generalized Fermat's Principle allows to determine if a ray path  
 308 represents a physical wave propagation and is consequently valid. Indeed this principle  
 309 indicates that the valid ray path for a wave resulting from particular interactions between the

310 wave field and surfaces and is the one providing the stationary time of flight and respecting  
311 the predefined conditions imposed to the wave propagation (choice of the modes for  
312 instance). This principle is verified by finding the minimal time of flight and the associated  
313 ray path. Consequently the principle of the GIRT is to find the valid ray path respecting the  
314 Generalized Fermat's principle and achieving the wave propagation conditions using a time of  
315 flight minimization technique. Its algorithm process is described in the following section.

316

#### 317 **2.4. GIRT algorithm process**

318

319 The steps of GIRT algorithm process are described in this section for the general case of  
320 anisotropic media and schematically represented in the functional diagram of *Fig. 7*. This  
321 algorithm process is the subject of a patent filing [38].

322 This process is first described when used for determination of the head wave path, the first  
323 arrival (like the paths 1 on *Fig. 6a* and *Fig. 6b*) and is called in that case GIRT-A. The input  
324 data (step 1) of the GIRT are the CAO description of the specimen in which the ray path has  
325 to be calculated, the source and observation points which are the ray extremity points, the  
326 slowness surfaces for the wave propagation mode desired inside and outside the specimen, the  
327 description of defects inside the specimen and the discretization fineness of the specimen or  
328 flaw surfaces which defines the calculation accuracy.

329 Indeed the next steps of the algorithm process is the discretization of both each specimen  
330 surface (step 2) and of each existing defect (step 3) in order to deal with any irregular surface:  
331 for the configuration of *Fig. 6a*, the two irregular surfaces and the planar defect are meshed.

332 The obtained discretization points collection  $\{M_i\}_{i \in \{1, \dots, N\}}$  constitutes the secondary sources  
333 collection for waves diffraction as stated by the Huygens principle in a propagation medium  
334 constituted of homogeneous volumes. Consequently these secondary sources are possible  $M_i$

335 points composing the ray path as described in section 2.3. The GIRT at this step 2 uses a  
336 similar approach to the interface source method (ISM) developed by Zhang and al [35] since  
337 interface points are seen as secondary sources.. On the other hand, the discretization carried  
338 out by GIRT differs from that performed by ISM [35] and other SPM algorithms [29]. Indeed  
339 as only the surfaces and the defects are discretized, the ray path searching is done only  
340 through secondary sources located along the specimen and defects surfaces and not through a  
341 grid covering all the specimen volume. The obtained secondary sources collection has a  
342 limited size  $N$  compared to that generated from a volume discretization and provide a more  
343 stable and faster research of ray paths.

344 To determine the valid secondary sources involved in the searched ray path in the view of  
345 the two points ray tracing problem, the elementary paths between two secondary sources are  
346 calculated (step 4): an elementary path represents the wave propagation along a direct path  
347 involving two and only two  $M_i$  secondary sources without any other diffraction effect. All  
348 the valid elementary paths between two  $M_i$  points respecting the previous condition are  
349 calculated for all the  $M_i$  points and the associated elementary times of flight are deducted  
350 from the slowness surfaces given and stored by the algorithm process (step 5). As an example,  
351 the ray  $M_2M_5$  in *Fig. 6b* is an elementary ray path of the path 1 and path 2.

352 A secondary sources collection, an elementary paths collection and an associated  
353 elementary times of flight collection have been obtained during the previous steps. The  $M_s$   
354 source and  $M_o$  observation points are added in step 6 to the existing secondary sources  
355 collection and all the new valid elementary paths involving one of these two points are  
356 calculated and taken into account in the collections. The interest of having separated this step  
357 6 from step 5 is to allow the ray path calculation for different couples of source and  
358 observation points but with the same specimen without needing to recalculate at each ray

359 calculation all the other elementary paths in the specimen (already independently determined  
360 at step 5).

361 Finally, knowing the secondary sources collection and the elementary paths collection, the  
362 search for the valid wave ray path in the view of the two point ray tracing reduces to an  
363 optimization problem. It indeed corresponds to the determination of which secondary sources  
364  $M_i$  are involved in the ray path and then which elementary rays  $(M_j M_l)_{(j,l) \in (1,\dots,N)^2}$  compose  
365 the ray path associated to the minimal time of flight. This approach is called the Shortest Path  
366 Method (SPM) [29] in the seismic domain and is applied in the GIRT (step 7). The secondary  
367 source points collection are the nodes of an oriented graph. In this graph, two different  
368 vertices are connected by an elementary ray path included in the collection. At each path is  
369 associated a cost which is the elementary time of flight between of the path. Once the graph is  
370 obtained, the optimal route (leading to the shortest time of flight between the source and  
371 observation points) is obtained by the classical Dijkstra algorithm [39], which has the major  
372 advantage to be a fast route search algorithm since all possible routes are not calculated: only  
373 the most likely optimal routes are taken into account. At that step, the GIRT algorithm differs  
374 strongly from the ISM developed by Zhang and al [35]. ISM is conceived to perform ray  
375 shooting in a grid meshing all the volume by launching rays from a source in all directions  
376 and by propagating first arrival waves from nodes to nodes in the grid: consequently a ray  
377 path reaching a predefined observation point cannot be found directly notably if this point is  
378 not a grid node. In GIRT, the application of the Dijkstra algorithm on the secondary sources  
379 collection is well fitted and specific of the two point ray tracing problem. Indeed, the source  
380 and observation points have been integrated in the secondary sources collection so that the  
381 fast route search gives directly the valid ray path between these two points.

382 Later arrival waves (for example all paths represented in *Fig. 6a* and *Fig. 6b* except the  
383 paths 1) can also be modeled by a GIRT-B version by adding constraints on the searched ray

384 path, fixing one or more points through which the ray path must pass. In the case of a ray path  
385 calculation with obligatory points of passage, the GIRT-B process differs from that previously  
386 described for the head wave ray path (GIRT-A process) only by some slight changes. First,  
387 the GIRT-B inputs include in addition the list of sorted constraint points and the definition of  
388 independent types of wave propagation along each path connecting these points. Then the  
389 GIRT-B operates as follows: a couple of points is formed by the source point and the first  
390 constraint point, then several other couples by two adjacent constraint points and the last  
391 couple by the last constraint point and the observation point. An optimized ray is then  
392 searched between the two points of each couple: in that aim, the previous points are seen as  
393 the source and observation points for GIRT-A process and the GIRT-A process is  
394 consequently carried out independently for each couple, the latter having its own type of  
395 propagation, allowing all type of wave propagation in the specimen. At last, all the calculated  
396 couples ray paths are concatenated to obtain the complete ray path between the source and  
397 observation points.

398

### 399 **2.5. GIRT capabilities**

400

401 GIRT is thus a generic algorithm calculating geometrical paths and the corresponding ray  
402 time of flight propagating in isotropic or anisotropic media. It has been designed to determine  
403 the valid ray path between two points assuming one or several given interactions between the  
404 current ray and the irregular surface. The two points can be located anywhere inside or  
405 outside the specimen.

406 Two kinds of interactions, accounted by GTD [37], are supported by GIRT: diffraction on  
407 smooth objects, leading to surface creeping rays (see the ray  $M_5M_6$  on *Fig. 6b*), and  
408 diffraction on wedges or edges (see *Fig. 6a*), leading to bulk or surface diffracted rays.

409 Furthermore, the propagation of numerous wave modes is taken into account with potential  
410 mode conversion at the surface: the longitudinal and transversal modes (possibly occurring  
411 for different kinds of waves: bulk waves, lateral waves, reradiated head waves or surface  
412 waves...), and the surface Rayleigh-like waves.

413 All the ray paths presented on *Fig. 6a* and *Fig. 6b* are modeled by setting some wave  
414 propagation conditions supported by the GIRT. As an example the head wave ray paths 1 of  
415 *Fig. 6a* and *Fig. 6b* are calculated using by finding the shortest ray path for a longitudinal  
416 bulk wave without mode conversion. The ray path 2 of *Fig. 6a* is found for the condition of a  
417 wave propagation with the shortest time of flight and a mode conversion from L bulk to T  
418 bulk on the surface irregularity. The ray path 3 of *Fig. 6a* and the ray path 2 of *Fig. 6b* are  
419 modeled imposing a surface propagation condition (detailed in the comments of *Fig. 14*) to  
420 the ray path in order to propagate lateral waves along the specimen surface. Similarly the ray  
421 path 4 of *Fig. 6a* and ray path 3 of *Fig. 6b* are found using the same surface propagation  
422 condition and that of a wave mode conversion from a lateral wave to a Rayleigh wave. Finally  
423 the ray path 5 of *Fig. 6a* is calculated using a reflection condition on the internal surface and  
424 an obligatory point of passage  $M_8$  on the defect edge.

425 Thanks to the previously described capabilities, all the interactions occurring in the case of  
426 an irregular surface and presented in this section are modeled by GIRT. In next Part 3 of this  
427 paper, GIRT is applied to the head wave path modeling in TOFD near irregular surfaces and  
428 only the waves which may be responsible of the head wave propagation or examples of the  
429 least later arrival waves are studied. It is shown in Part 3 that GIRT provides accurate  
430 predictions for the time of flight and wave fronts of both the head wave and even later  
431 propagation waves in TOFD near irregular surfaces.

432

### 433 3. GIRT simulated results and theoretical validations

434

435 Calculations using GIRT of ray paths and wave fronts are shown in this section in the aim of  
436 modeling the propagation of head waves near irregular surfaces in some TOFD  
437 configurations. Such simulations are compared and superimposed to FEM ones.

438

#### 439 3.1. Validation of the head wave time of flight

440

441 A theoretical validation of GIRT is performed by comparing times of flight calculated with  
442 both GIRT and finite-elements (FEM) simulations obtained with CIVA/Athena, which is  
443 considered here as a reference model. The comparison deals with TOFD inspection  
444 simulations for several inspection directions ( $\theta = 45^\circ, 60^\circ$  and  $75^\circ$  where  $\theta$  is the angle  
445 defined in *Fig. 8*) with L waves emitted at 5MHz. The specimen is a planar stainless steel  
446 block which is inspected using two contact planar rectangular transducers (6mm\*5mm). The  
447 specimen entry surface has two slopes. The head wave path determined by GIRT is illustrated  
448 in blue in *Fig. 8* and includes a diffraction on the surface corner.

449 The times of flight obtained by GIRT have been compared to the results of the FEM  
450 simulation software for different slope angles and are shown in *Fig. 9*. Each graph of the *Fig.*  
451 *9* is associated to a particular inspection direction (from  $L45^\circ$  to  $L75^\circ$ ), the solid lines are the  
452 results obtained with the GIRT and the dashed lines are the results obtained by FEM  
453 simulations.

454 The graphs show a very good concordance between the results of the GIRT and FEM  
455 simulation, for each direction of inspection and any slope angle. The GIRT is then able to  
456 calculate the head wave time of flight with a very good precision (error less than 0.1%). The  
457 simulated times of flight of the head wave signal received by the probe are almost

458 independent of the inspection directions because the head wave signal is generated by only  
459 some refracted rays included in the beam radiated in the specimen by the emitter surface,  
460 those rays being close to the mean head wave path shown in blue in *Fig. 8* including a  
461 diffraction on the corner.

462

### 463 **3.2. Analysis of the propagation of waves in the surface shadow**

464

465 Additional finite-element simulations on CIVA/Athena have been performed on irregular  
466 surfaces including curved parts, and the propagation wave field in the material at different  
467 times is also visualized on FEM snapshots. In this section, GIRT has been employed in the  
468 aim of identifying the nature of waves propagation corresponding to some observed  
469 wavefronts in the FEM snapshots.

470 Indeed, when studying the interaction on a beam with an irregular surface, numerous wave  
471 fronts are generated. For instance *Fig. 10* shows FEM simulation of the waves propagation  
472 near a curved valley constituted of two curved edges separated by a planar part. Numerous  
473 wave fronts are observed in the FEM snapshot of *Fig. 10*, which highlights the great number  
474 of interactions occurring between the refracted field and the specimen. The nature of some of  
475 these wave fronts (numerated in *Fig. 10*) can be easily guessed. The surrounded front L1  
476 corresponds to the direct L-wave refracted in the specimen by the emitter. The front L1 is  
477 reflected by the specimen bottom (dashed black horizontal line in *Fig. 10*) creating the L-  
478 wave front L2 and T-wave front T1. T2 refers to T-waves refracted in the specimen. Other  
479 wave fronts are of more complex nature. It is consequently of interest to identify the nature of  
480 rays which have generated the observed wave fronts in the FEM simulations.

481 So as to identify the nature of one particular FEM wave front, the following methodology  
482 is chosen:

- 483 - The studied wave front is identified on the FEM snapshot as the local maximum of the  
484 displacement field.
- 485 - An appropriate hypothesis on the wave propagation and interactions with the surface is  
486 formulated by the GIRT user to explain the generation of the studied wave front.
- 487 Considering the previously chosen path hypothesis, GIRT builds rays until their time of  
488 flight reach the FEM snapshot time.
- 489 - The resulting wave front simulated by GIRT is then drawn for the FEM snapshot time  
490 by tracing the curve orthogonal to every ray found at this time of flight [40]. The GIRT  
491 simulated wave front is superimposed to the FEM snapshot and its location compared  
492 to that of the FEM studied wave front to validate the chosen propagation hypothesis.

493 In the present study, identification of wave fronts nature by comparing FEM and GIRT  
494 simulations is done only for wave fronts relevant for studying head waves propagation. But a  
495 similar analysis could be performed for all the other wave fronts observed on FEM snapshots.  
496 The method is thus applied for the following wave fronts:

- 497 - The front of the refracted L-wave (*Fig. 10*), whose diffraction on the second curved  
498 part of the surface specimen is responsible of head wave propagation towards the  
499 receiver (as said in section 2.2).
- 500 - The L head wave (*Fig. 11 and 13*), received at first on the receiver.
- 501 - The T wave received just after the L head wave on the receiver.

502 For each figure, the ray paths (white lines) and the front (dashed black line) simulated by  
503 GIRT are superimposed to the studied FEM snapshot (in color code).

504 In *Fig. 10*, ray paths simulated by GIRT are obtained considering the hypothesis injected in  
505 GIRT of a diffraction of the refracted L-wave field on a curved object without mode  
506 conversion and without constraint point. Ray paths are thus built with the GIRT-A algorithm  
507 between one source point (emitter center) and a set of observation points located in the

508 specimen bulk after the second curved part at right, inside the shadow areas formed by the  
509 surface irregularity. The GIRT objective is here to determine between the source and each  
510 observation point the shortest path which corresponds to the head wave path. The calculated  
511 ray path indicates that the emitted wave is refracted in the specimen bulk, before being  
512 diffracted by the first curved object at left. The GIRT modeling of the diffracted field by near  
513 this curved part reveals creeping rays. Indeed, the refracted longitudinal rays reaching  
514 tangentially the first curved object are converted into creeping rays. These creeping rays are  
515 then diffracted into both bulk rays along their curved propagation and a surface ray which  
516 propagates along the planar surface. The surface ray is converted again at the junction with  
517 the second curved part into a creeping ray which is diffracted into bulk rays generated  
518 tangentially to the second curved object at right inside the shadow area caused by the surface  
519 irregularity. As seen in *Fig. 10*, the calculated wave front is the result of the wave diffractions  
520 on the two curved objects. The previously described head wave propagation is validated by  
521 comparing the GIRT and FEM simulated wave fronts and observing a good agreement  
522 between them.

523 The following two cases, presented in *Fig 11* and *Fig 12* are obtained with the same  
524 configuration as in *Fig. 10*, but the propagation of waves is extended up to the receiver,  
525 allowing observing the wave fronts received in experimental studies. As in *Fig. 10*, the  
526 refracted longitudinal wave is diffracted by the curved parts at left and at right and refracted  
527 again at the last surface between the specimen and the wedge of the receiving probe. Two  
528 different hypotheses detailed hereafter are inputted in GIRT concerning the second refraction  
529 (at the interface specimen/wedge of the receiver) and give the results of respective *Fig. 11* and  
530 in *Fig. 12*. In *Fig. 11*, a second refraction of longitudinal waves without mode conversion is  
531 assumed and GIRT-A is used to calculate the shortest rays between the source an observation  
532 points located on the receiver crystal surface. In *Fig. 12*, a second refraction with conversion

533 of the L wave into a T wave is supposed. To apply the last hypothesis, a constraint point is  
534 defined on the plane part of the irregularity and the GIRT-B algorithm is used so as to  
535 calculate the rays using the following assumptions: when the path takes place inside the  
536 specimen, it is always travelled at the celerity of the L wave; when the path takes place both  
537 outside the specimen and from the source point to the constraint point (i.e. in the emitter  
538 wedge), it is travelled at the celerity of the L wave; when the path takes place both outside the  
539 specimen and from the constraint point to the receiver point (i.e. in the receiver wedge), it is  
540 travelled at the celerity of the T wave. By this way ray paths calculated by the GIRT-B satisfy  
541 the mode conversion L-T condition on the surface near the receiver. As in *Fig. 10* and for the  
542 two cases in *Fig. 11* and *Fig. 12*, wave fronts calculated by GIRT perfectly match with two  
543 different wave fronts simulated by FEM. Furthermore the wave of type T (*Fig. 12*) is received  
544 by the receiver later than that of type L (*Fig. 11*) as shown by comparing the location of their  
545 corresponding wave fronts for a fixed time of flight. Consequently, in the previous  
546 configuration, the head wave observed at the receiver which is by definition the first received  
547 wave logically mainly corresponds to a complete path without mode conversion involving  
548 only faster L waves. All the other FEM simulated wave fronts obtained in the snapshot of *Fig.*  
549 *11* lead to later arrival times if they reach the receiver.

550 To emphasize this conclusion about the nature of the head wave propagation, the GIRT  
551 simulated rays of a L-surface wave propagation all along the irregular specimen surface  
552 without any specimen bulk propagation hypothesis are shown in *Fig. 13*. To satisfy the  
553 previous condition, two constraints points are specified to the GIRT-B algorithm and are  
554 positioned on the specimen surface respectively just before and just after the surface  
555 irregularity, so as to impose the propagation of rays along the irregular surface. In that case,  
556 the surface ray is generated by critical incidence on a planar interface as described in *Fig. 1*.  
557 The corresponding extracted wave front does not match the head wave front obtained from

558 FEM simulations and confirms that the bulk mechanism stated previously for the head wave  
559 propagation is likely to predominate for very corrugated surfaces.

560 The results in the previous comparisons between GIRT and FEM show that the head wave  
561 propagation in the bulk implied by complex interactions between the wave and the surface  
562 must be taken into account to correctly model the head wave propagation on irregular  
563 surfaces. These comparisons between the developed ray tracing model (GIRT) and FEM  
564 simulations validate the choice of the GTD approach used in GIRT to model the complex  
565 interactions between an irregular surface and the waves radiated by the probe. The GIRT  
566 based on GTD principles is able to compute valid ray paths providing wave fronts in  
567 agreement with FEM simulated results in terms of both location and shape.

568

#### 569 **4. Conclusion**

570

571 The modeling of TOFD configurations used in ultrasonic NDT requires the study of the  
572 head wave propagation. While analytical theories for head waves on planar interfaces are well  
573 established, the complete simulation of head waves on irregular surfaces has to be developed.  
574 In that aim, one suitable approach is to use the Geometrical Theory of Diffraction.

575 A generic algorithm of ray tracing between interface points (GIRT) has thus been  
576 developed using one GTD principle: the Generalized Fermat's Principle. GIRT is a specific  
577 and generic adaptation of seismic ray tracings to NDE modeling of waves propagation and to  
578 the two points ray tracing problem solving: a fast processing of the waves propagation near  
579 very irregular surfaces between two fixed points is obtained by meshing only those surfaces  
580 and the defects rather than all the volume of the propagation media like in existing seismic ray  
581 tracings. The approach is adequate for a propagation medium constituted of homogenous or  
582 weakly inhomogeneous volumes: in the latter case, the wave propagation can be modeled by

583 tracing straight lines in a mean homogenous volume and adding travel time fluctuations [41].  
584 The advantages of the GIRT are the specific treatment of diffracted and creeping rays in  
585 shadow areas, the account of both any irregular surfaces of the specimen and embedded  
586 defects (both CAD defined), the wave mode conversions at interfaces or flaws, and the  
587 calculation of all waves (bulk, surface and head waves) propagating towards a predefined  
588 observation point during a TOFD inspection for NDE including both first arrival (head wave)  
589 and latter arrival waves.

590 By modeling the complex wave interactions with the surfaces thanks to this ray approach,  
591 GIRT is able to correctly predict the head wave time of flight and to interpret the complex  
592 waves propagation at the vicinity of an irregular interface. For very corrugated surfaces, a  
593 bulk propagation mechanism has to be taken into account for the head wave modeling.

594 Valid geometrical rays paths are henceforth determined for head waves using GIRT pure  
595 kinematic analysis. Use of GTD for simulation of the head wave amplitude will be  
596 investigated thereafter by modeling surface creeping rays and corner diffractions. GIRT could  
597 then lead in the future to a complete modeling of the head wave propagation on irregular  
598 interfaces.

599

## 600 **References**

601

- 602 [1] L.M. Brekhovskikh, Waves in layered media, Academic press New York, 1960.  
603 [2] K. Friedrichs, J.B. Keller, Geometrical acoustics. II. Diffraction, reflection, and  
604 refraction of a weak spherical or cylindrical shock at a plane interface, J. Appl. Phys. 26  
605 (1955) 961–966.  
606 [3] V. Červený, R. Ravindra, Theory of seismic head waves, University of Toronto Press  
607 (Toronto), 1971.  
608 [4] L. Cagniard, E.A. Flinn, C.H. Dix, W.G. Mayer, Reflection and Refraction of  
609 Progressive Seismic Waves, Phys. Today. 16 (1963) 64.  
610 [5] A. De Hoop, A modification of Cagniard's method for solving seismic pulse problems,  
611 Appl. Sci. Res. Sect. B. 8 (1960) 349–356.  
612 [6] H. Uberall, Surface waves in acoustics, in Physical Acoustics 10 (W. P. Mason  
613 and R. N. Thurston, eds.), Academic Press, New York (1973) pp. 1-60.

- 614 [7] J. Goodier, R. Bishop, A note on critical reflections of elastic waves at free surfaces, *J.*  
615 *Appl. Phys.* 23 (1952) 124–126.
- 616 [8] S. Mahaut, M. Darmon, P. Benoist, P. Calmon, TOFD inspection simulation using Civa  
617 software, in: *Proc. BINDT*, 2007.
- 618 [9] S. Chaffai, M. Darmon, S. Mahaut, R. Menand, Simulation Tools for TOFD Inspection  
619 in CIVA Software, in: *Proc. 6th ICNDE*, 2007.
- 620 [10] Assessment, Management of ageing of major nuclear power plant components  
621 important to safety primary piping in PWRs, Vienna: IAEA, 2003.
- 622 [11] M. Darmon, S. Chatillon, S. Mahaut, L. Fradkin, A. Gautesen, Simulation of disoriented  
623 flaws in a TOFD technique configuration using GTD approach, in: *AIP Conf. Proc.*,  
624 2008: p. 155.
- 625 [12] V. Zernov, L. Fradkin, M. Darmon, A refinement of the Kirchhoff approximation to the  
626 scattered elastic fields, *Ultrasonics*. 52 (2012) 830–835.
- 627 [13] G. Huet, M. Darmon, A. Lhémy, S. Mahaut, Modelling of corner echo ultrasonic  
628 inspection with bulk and creeping waves, in: *Ultrason. Wave Propag. Non Homog.*  
629 *Media*, Springer, 2009: pp. 217–226.
- 630 [14] S. Mahaut, G. Huet, M. Darmon, Modeling of corner echo in UT inspection combining  
631 bulk and head waves effect, in: *AIP Conf. Proc.*, 2009: p. 73.
- 632 [15] H. Zhou, X. Chen, Ray path of head waves with irregular interfaces, *Appl. Geophys.* 7  
633 (2010) 66–73.
- 634 [16] I. Lerche, N. Hill, A mean-field solution of the reflection of a spherical acoustic wave  
635 from a rough interface, *J. Math. Phys.* 26 (1985) 1420.
- 636 [17] I. Lerche, On the reflection of acoustic waves from a slightly curved interface, *J.*  
637 *Acoust. Soc. Am.* 81 (1987) 611.
- 638 [18] D.P. Hill, Critically refracted waves in a spherically symmetric radially heterogeneous  
639 earth model, *Geophys. J. Int.* 34 (1973) 149–177.
- 640 [19] B. Julian, D. Gubbins, Three-dimensional seismic ray tracing, *J Geophys.* 43 (1977) 95–  
641 114.
- 642 [20] Y. Wang, G.A. Houseman, Tomographic inversion of reflection seismic amplitude data  
643 for velocity variation, *Geophys. J. Int.* 123 (1995) 355–372.
- 644 [21] Y. Wang, *Seismic amplitude inversion in reflection tomography*, Pergamon, 2003.
- 645 [22] V. Vinje, E. Iversen, H. Gjøystdal, Traveltime and amplitude estimation using  
646 wavefront construction, *Geophysics*. 58 (1993) 1157–1166.
- 647 [23] J. Vidale, Finite-difference calculation of travel times, *Bull. Seismol. Soc. Am.* 78  
648 (1988) 2062–2076.
- 649 [24] J.E. Vidale, Finite-difference calculation of traveltimes in three dimensions,  
650 *Geophysics*. 55 (1990) 521–526.
- 651 [25] K. Koketsu, others, Finite difference traveltime calculation for head waves travelling  
652 along an irregular interface, *Geophys. J. Int.* 143 (2000) 729–734.
- 653 [26] N. Rawlinson, M. Sambridge, Multiple reflection and transmission phases in complex  
654 layered media using a multistage fast marching method, *Geophysics*. 69 (2004) 1338–  
655 1350.
- 656 [27] M. De Kool, N. Rawlinson, M. Sambridge, A practical grid-based method for tracking  
657 multiple refraction and reflection phases in three-dimensional heterogeneous media,  
658 *Geophys. J. Int.* 167 (2006) 253–270.
- 659 [28] I. Nakanishi, K. Yamaguchi, A numerical experiment on nonlinear image reconstruction  
660 from first-arrival times for two-dimensional island arc structure, *J. Phys. Earth.* 34  
661 (1986) 195–201.
- 662 [29] T. Moser, Shortest path calculation of seismic rays, *Geophysics*. 56 (1991) 59–67.

- 663 [30] S. Cao, S. Greenhalgh, Calculation of the seismic first-break time field and its ray path  
 664 distribution using a minimum travelttime tree algorithm, *Geophys. J. Int.* 114 (1993)  
 665 593–600.
- 666 [31] H.J. Van Avendonk, A.J. Harding, J.A. Orcutt, W.S. Holbrook, Hybrid shortest path and  
 667 ray bending method for travelttime and raypath calculations, *Geophysics.* 66 (2001) 648–  
 668 653.
- 669 [32] A. Zhao, Z. Zhang, J. Teng, Minimum travel time tree algorithm for seismic ray tracing:  
 670 improvement in efficiency, *J. Geophys. Eng.* 1 (2004) 245.
- 671 [33] C. Bai, S. Greenhalgh, B. Zhou, 3D ray tracing using a modified shortest-path method,  
 672 *Geophysics.* 72 (2007) T27–T36.
- 673 [34] C. Bai, G. Huang, R. Zhao, 2-D/3-D irregular shortest-path ray tracing for multiple  
 674 arrivals and its applications, *Geophys. J. Int.* 183 (2010) 1596–1612.
- 675 [35] M.-G. Zhang, Y.-G. Jia, M.-Y. Wang, X.-F. Li, A global minimum travelttime ray  
 676 tracing algorithm of wavefront expanding with interface points as secondary sources,  
 677 *Chin. J. Geophys.* 49 (2006) 1046–1053.
- 678 [36] N. Gengembre, A. Lhémery, R. Omote, T. Fouquet, A. Schumm, A semi-analytic-FEM  
 679 hybrid model for simulating UT configurations involving complicated interactions of  
 680 waves with defects, in: *AIP Conf. Proc.*, 2004: p. 74.
- 681 [37] J.B. Keller, Geometrical theory of diffraction, *JOSA.* 52 (1962) 116–130.
- 682 [38] Patent filing related to GIRT in progress. Its precise reference will be given in the  
 683 proofs.
- 684 [39] E.W. Dijkstra, A note on two problems in connexion with graphs, *Numer. Math.* 1  
 685 (1959) 269–271.
- 686 [40] D. Bouche, F. Molinet, R. Mittra, *Asymptotic methods in electromagnetics*, Springer,  
 687 1997.
- 688 [41] B. Lu, M. Darmon, C. Potel, Stochastic simulation of the high-frequency wave  
 689 propagation in a random medium, *J. Appl. Phys.* 112 (2012) 054902–054902.

690  
 691

### Figure Captions

692

693 Figure 1: A NDT inspection using TOFD technique

694 Figure 2: Experimental B-scan observed in the TOFD inspection of Fig. 1

695 Figure 3: An irregular geometry studied by TOFD technique

696 Figure 4: TOFD inspection measurement on the specimen including a valley of finite

697 extension as described in Fig. 3. a): experimental B-scan obtained when scanning the  
 698 specimen in the extension direction (perpendicular to planes of Fig. 4b) and 4c). For the  
 699 first left scanning positions, the probes are on a planar part (Fig. 4b) and they are then  
 700 located on both sides of the valley (Fig. 4c).

701 Figure 5: Propagation of a HW on an irregular surface (valley consisting in several planar  
702 slopes). a) Theoretical propagation of the head wave. b) Snapshot of the field calculated  
703 by FEM at the location of the diffraction phenomena (in the yellow area of Fig 5a).

704 Figure 6: Various paths (color lines) resulting from several interactions with two kinds of  
705 surfaces (black lines): a surface with a corner irregularity (a) and a surface with a  
706 cylindrical irregularity (b).

707 Figure 7: Functional diagram of the GIRT algorithm process

708 Figure 8: TOFD inspection used for the theoretical validation of GIRT.

709 Figure 9: Comparison of times of flight calculated both with GIRT and with FEM simulations  
710 (Civa/Athena) versus slope angles for different inspection directions (a:  $45^\circ$ , b:  $60^\circ$ , c:  
711  $75^\circ$ ).

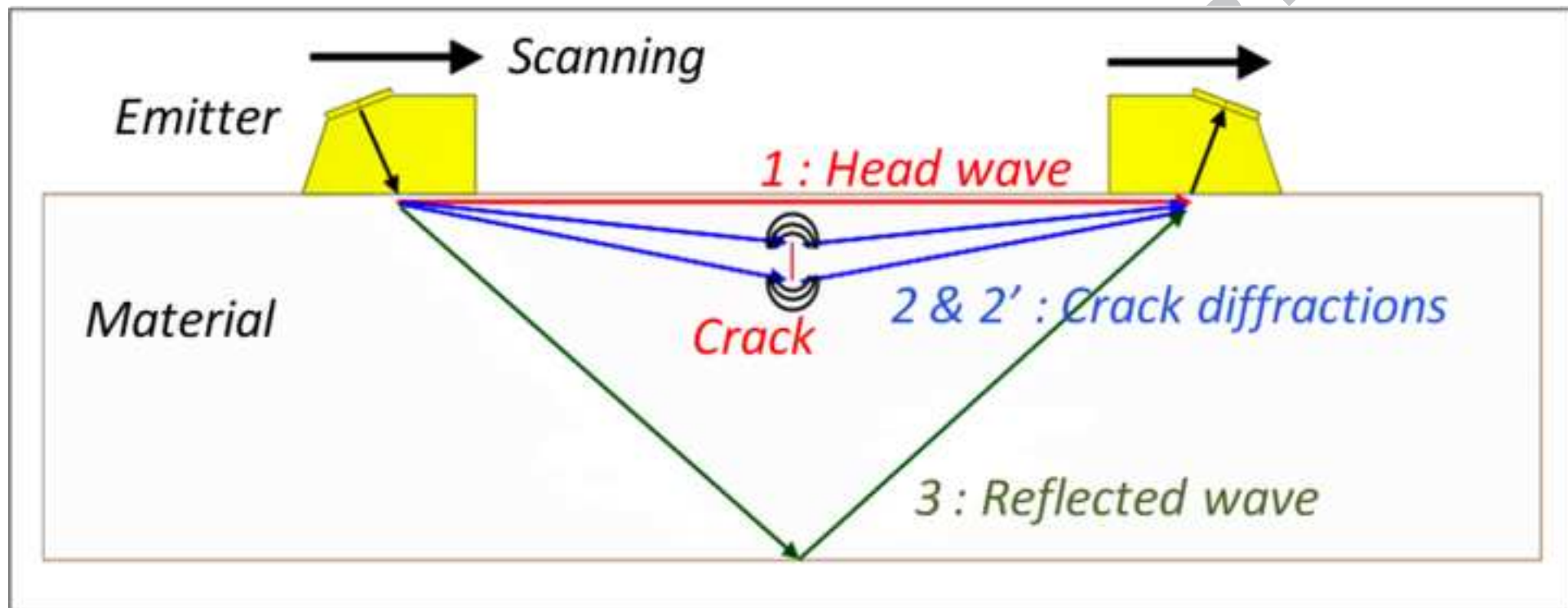
712 Figure 10: Diffraction of L-waves on curved objects. Head wave ray paths calculated by  
713 GIRT are represented in white and forms the simulated wave front in black. FEM  
714 simulated snapshot is in color code.

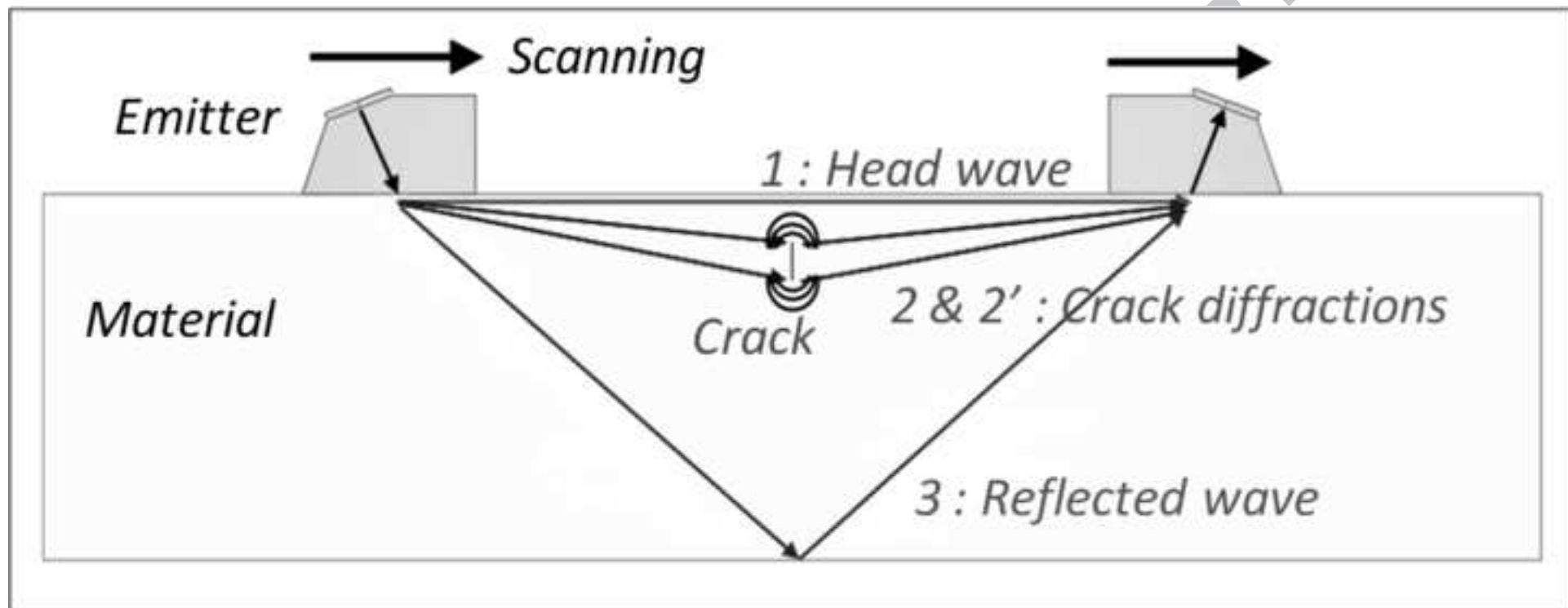
715 Figure 11: Head wave (L wave) received by the transducer. At right: zoom on the receiver.

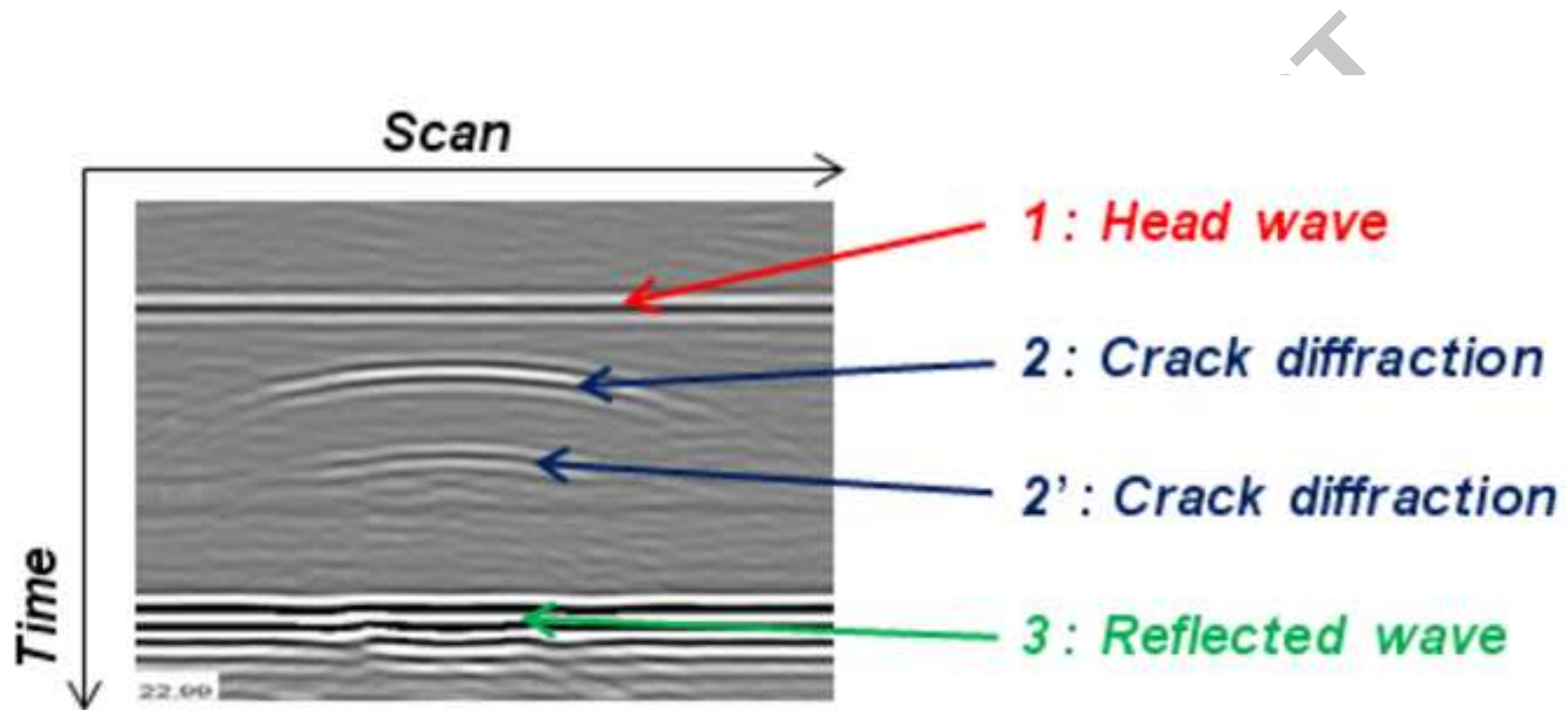
716 Figure 12: Hypothesis of a T wave received by the transducer. At right: zoom on the receiver.

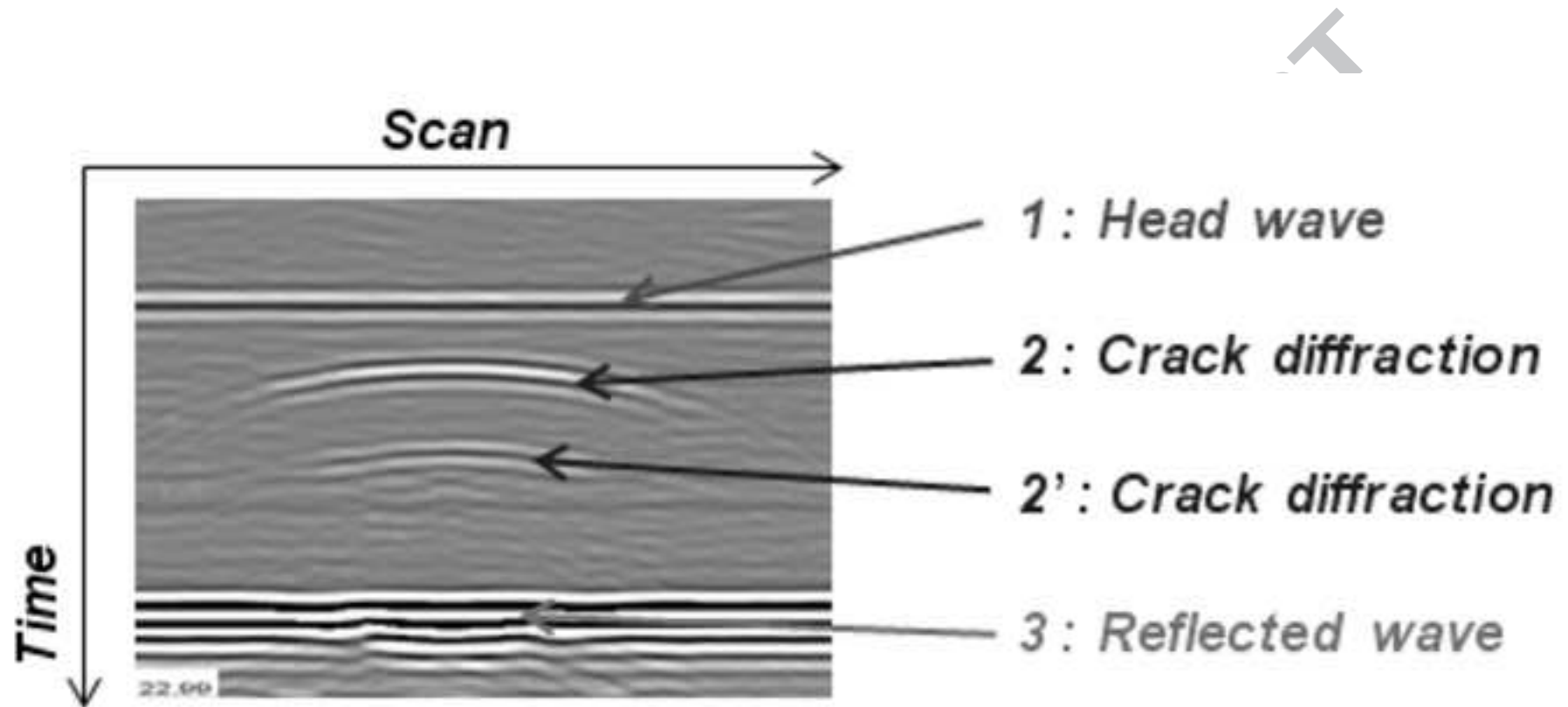
717 Figure 13: Hypothesis of a L wave received by the transducer without propagation in the  
718 specimen bulk. At right: zoom on the receiver.

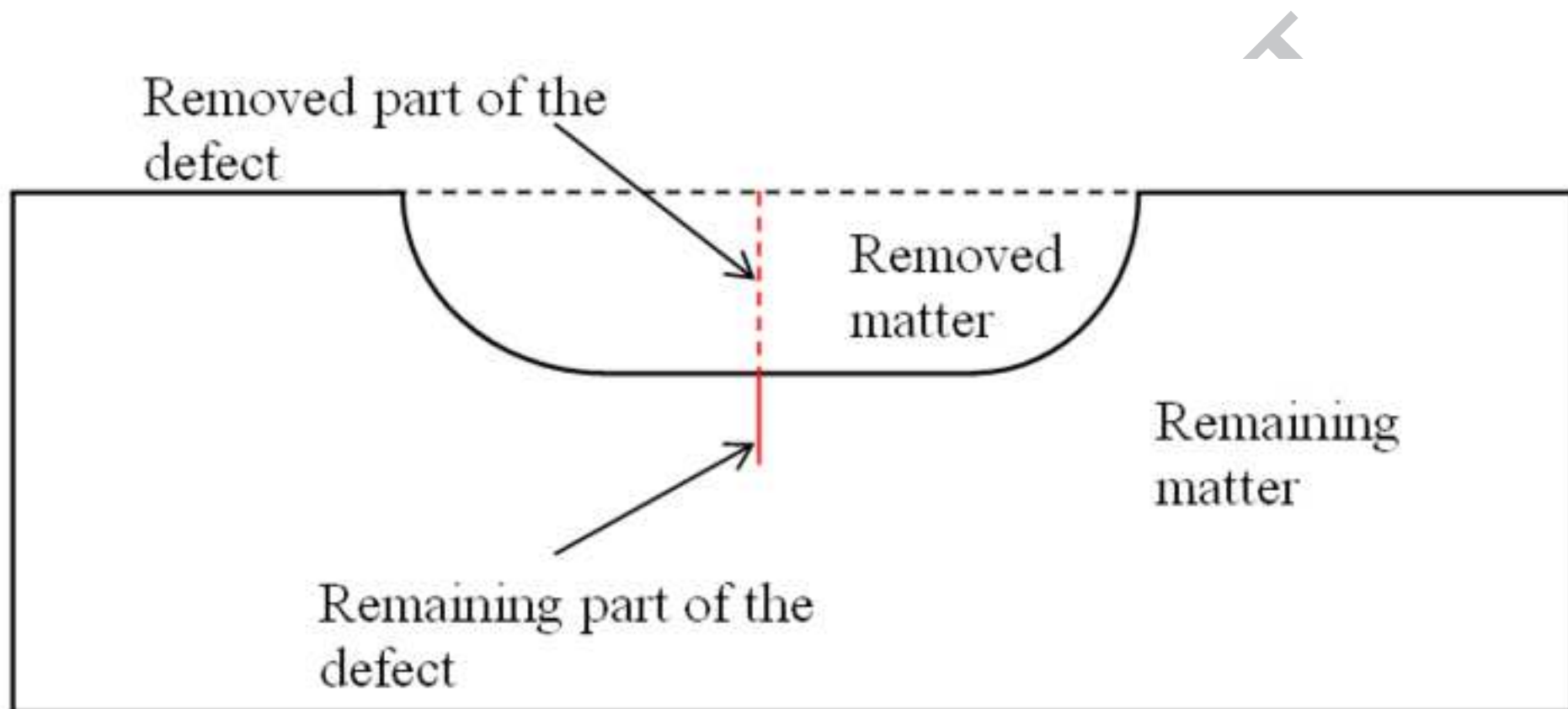
719

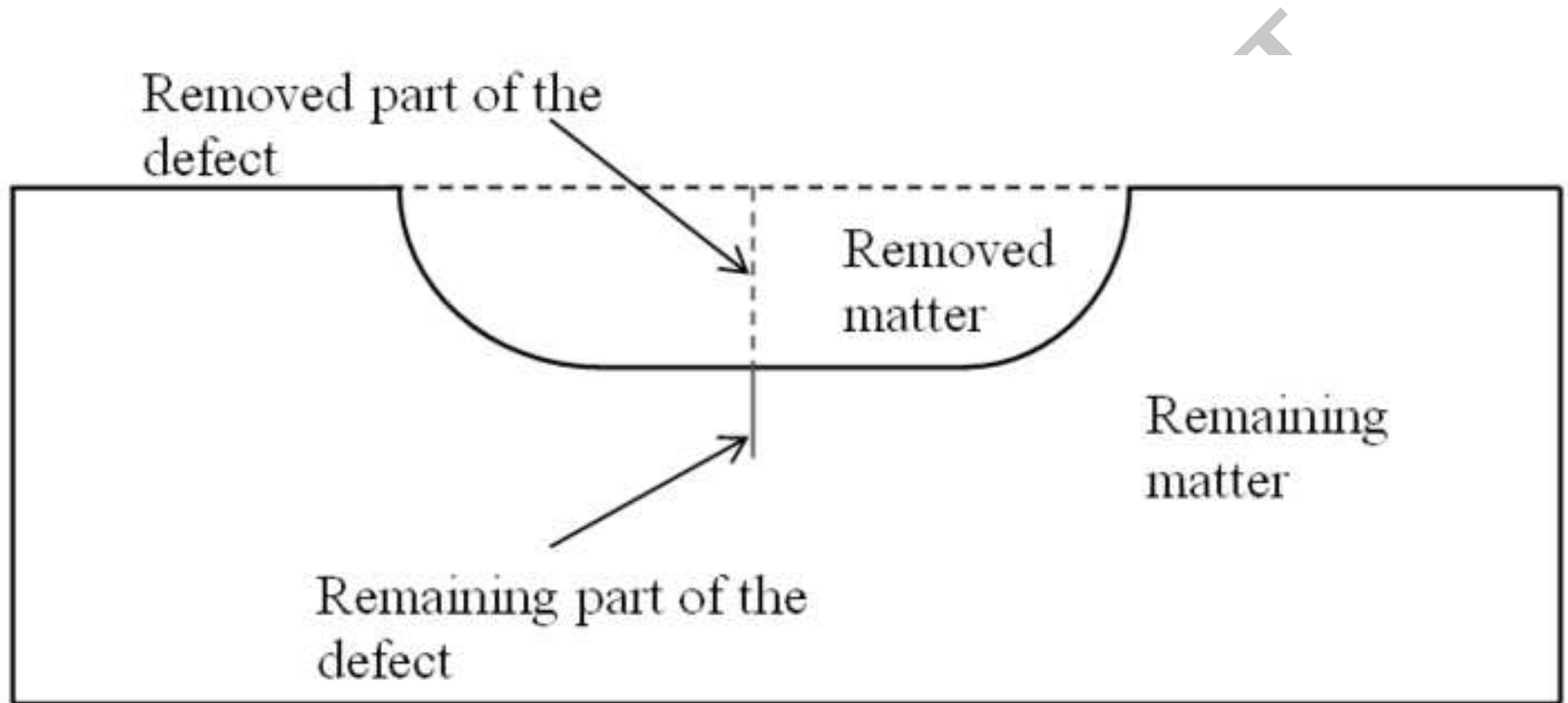


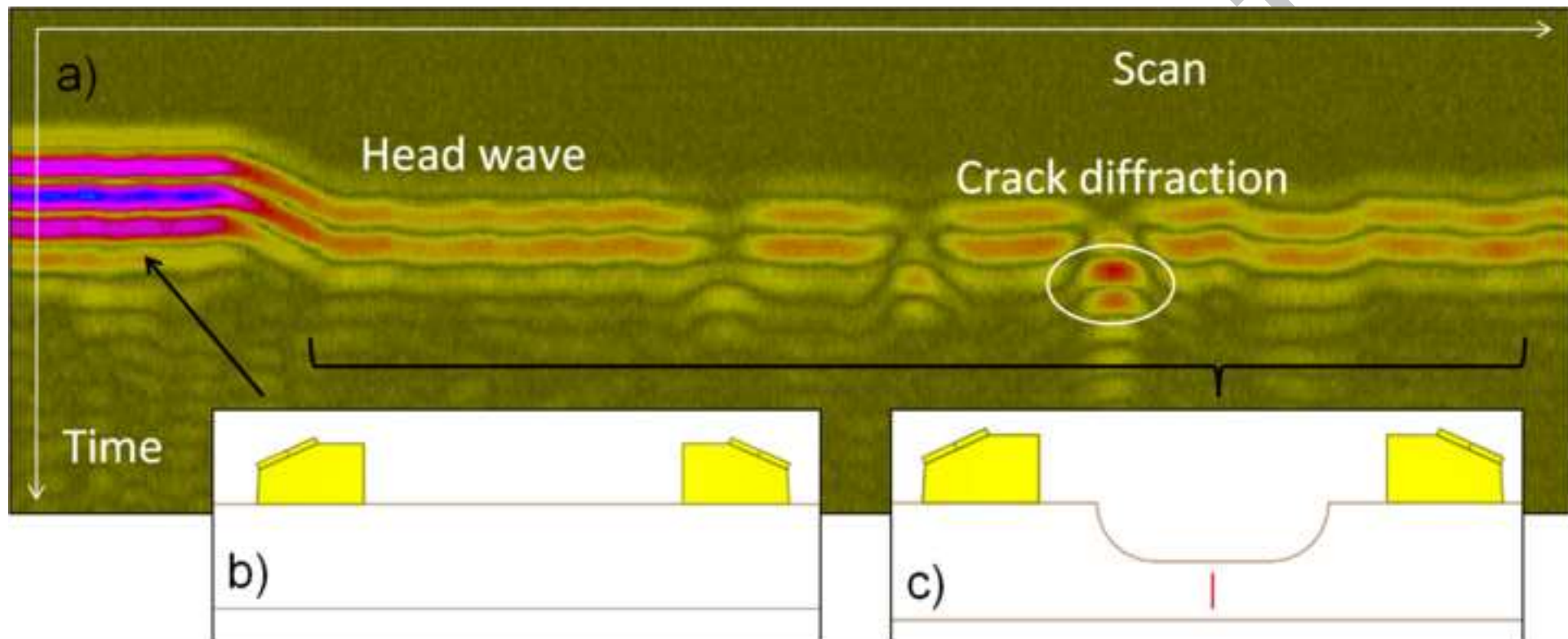


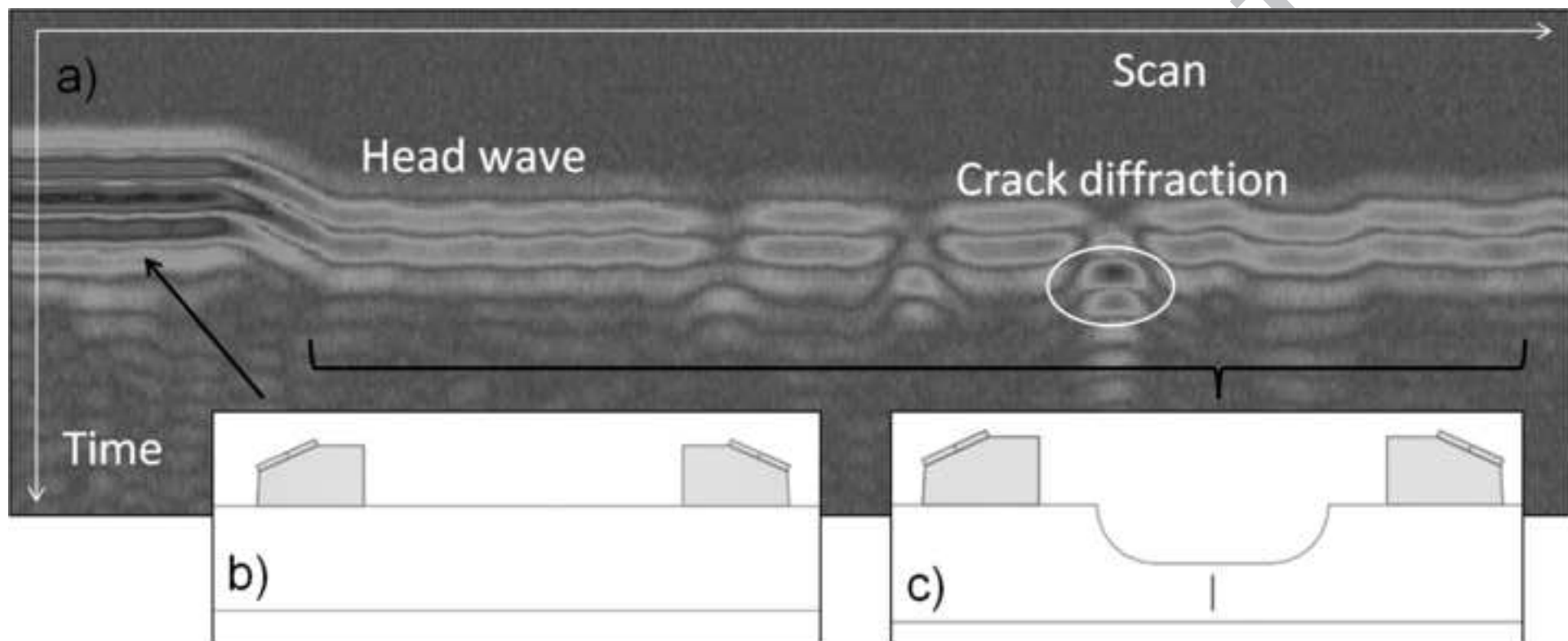


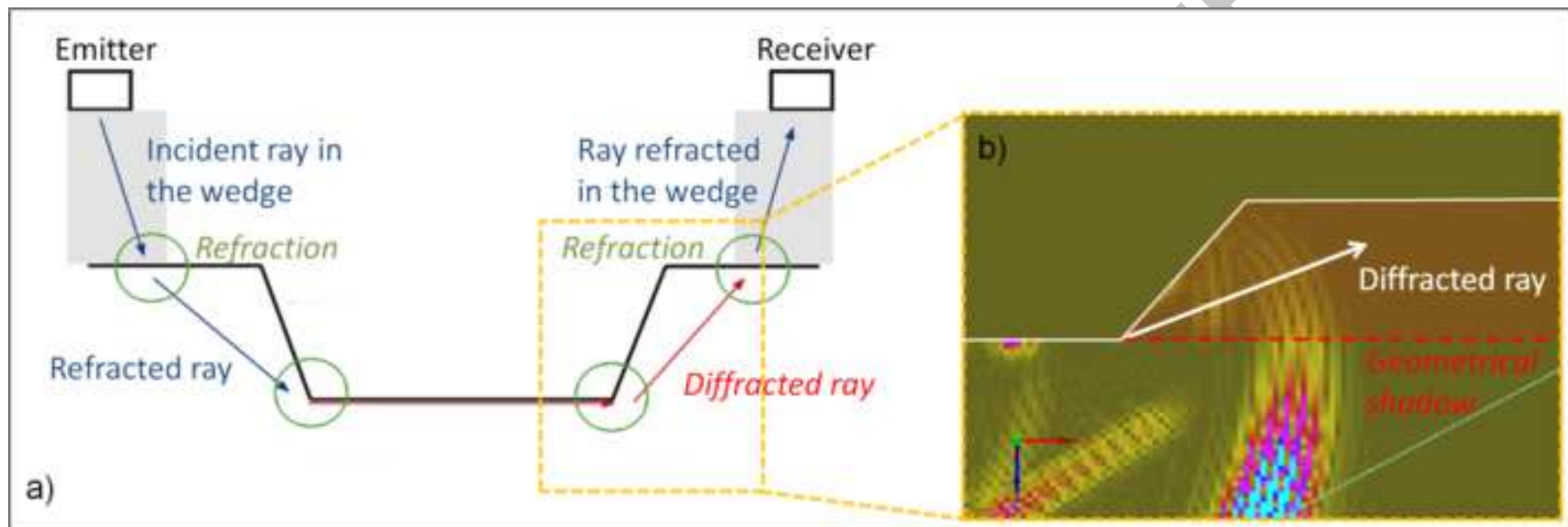












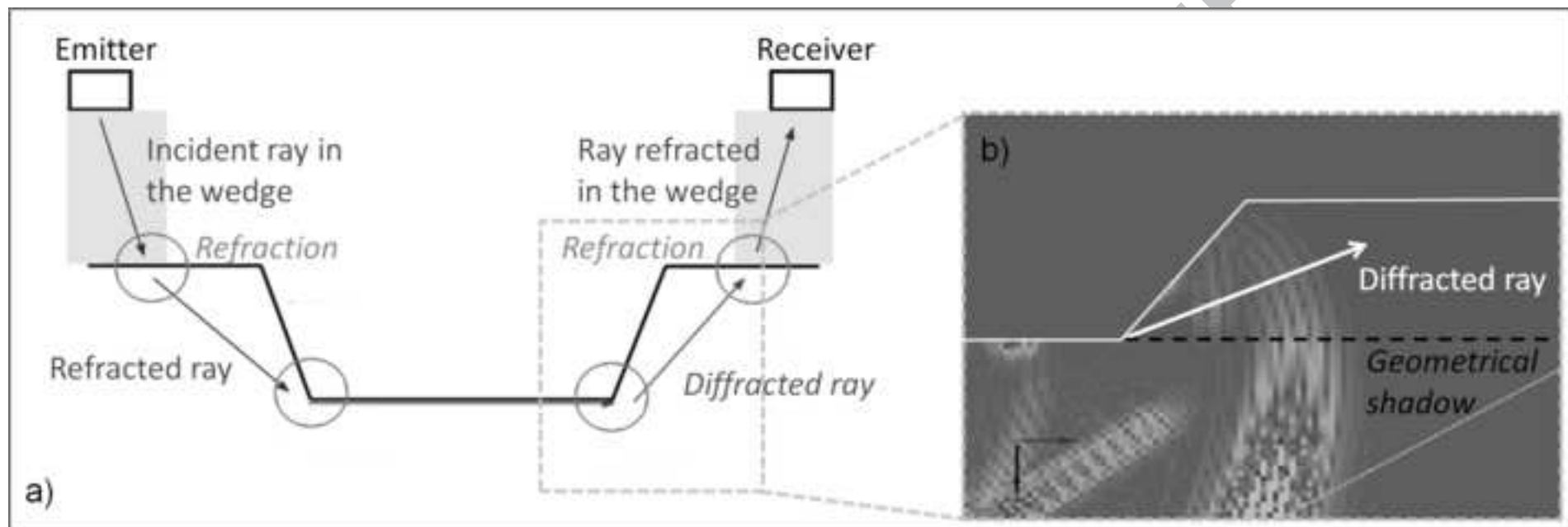
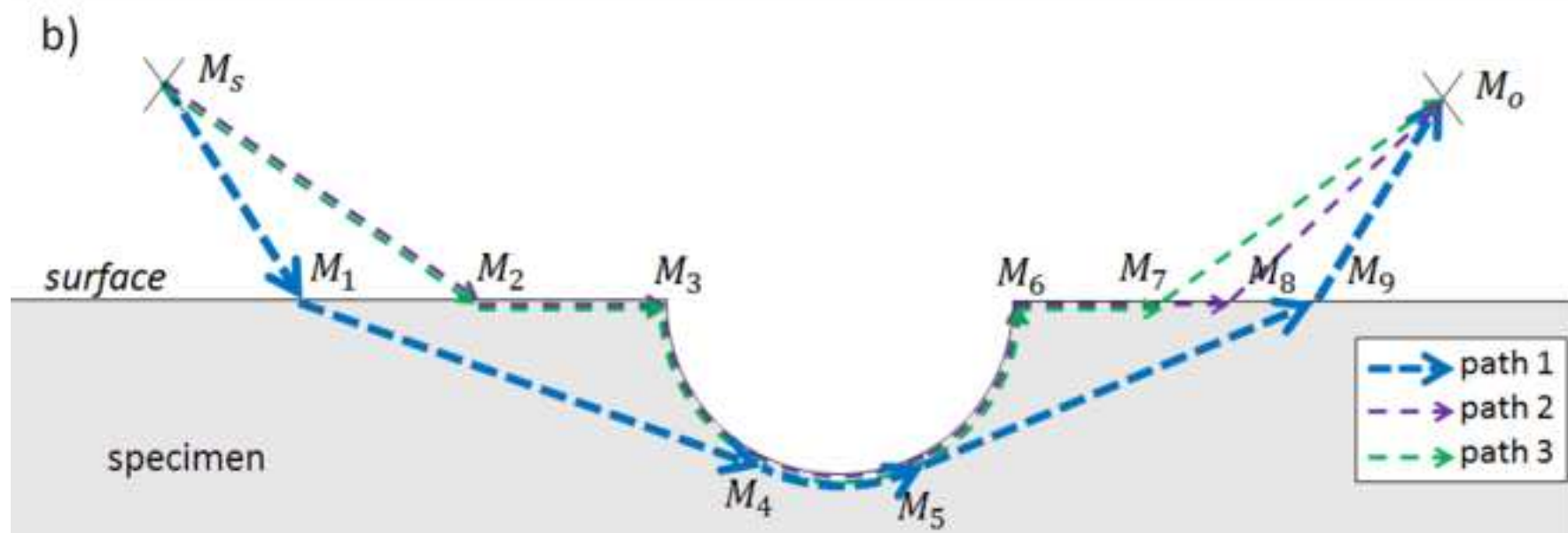
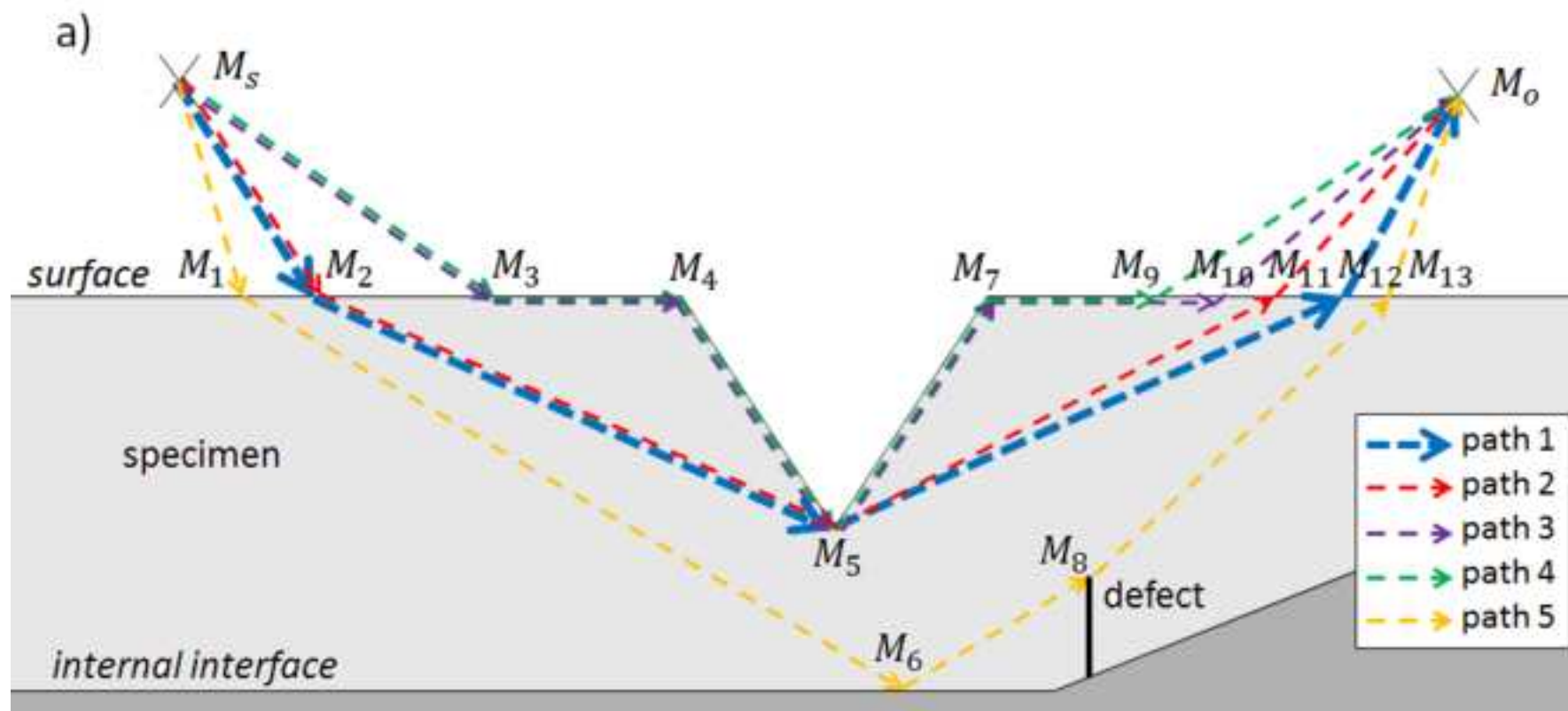


Figure 6



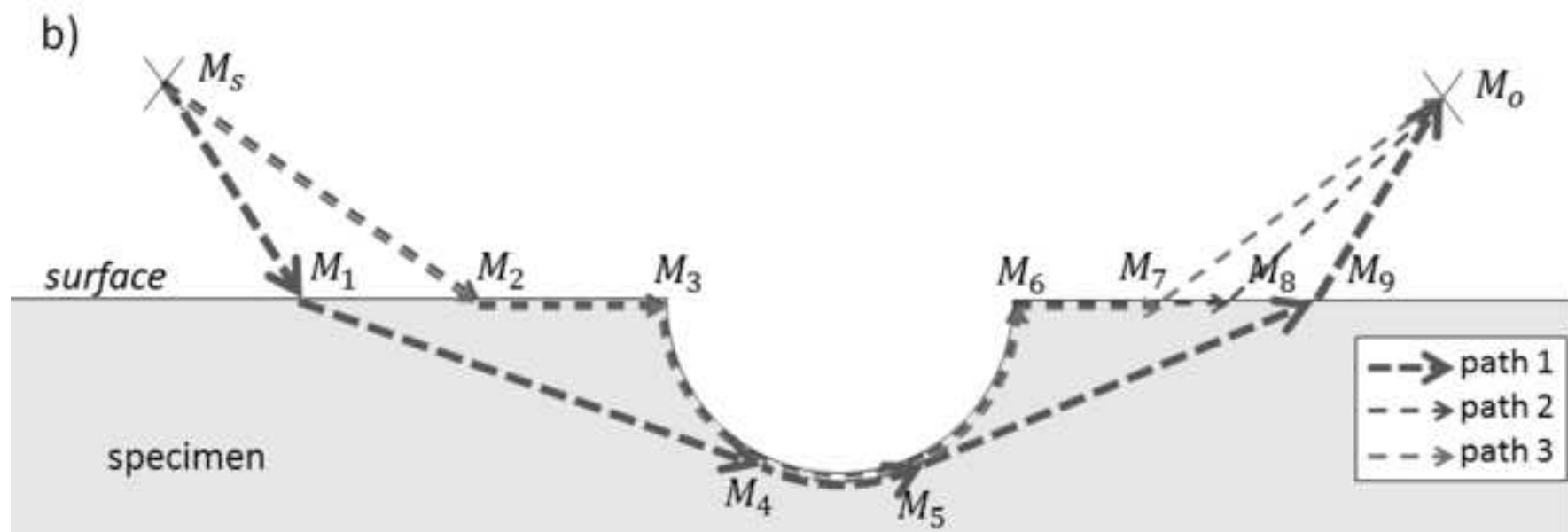
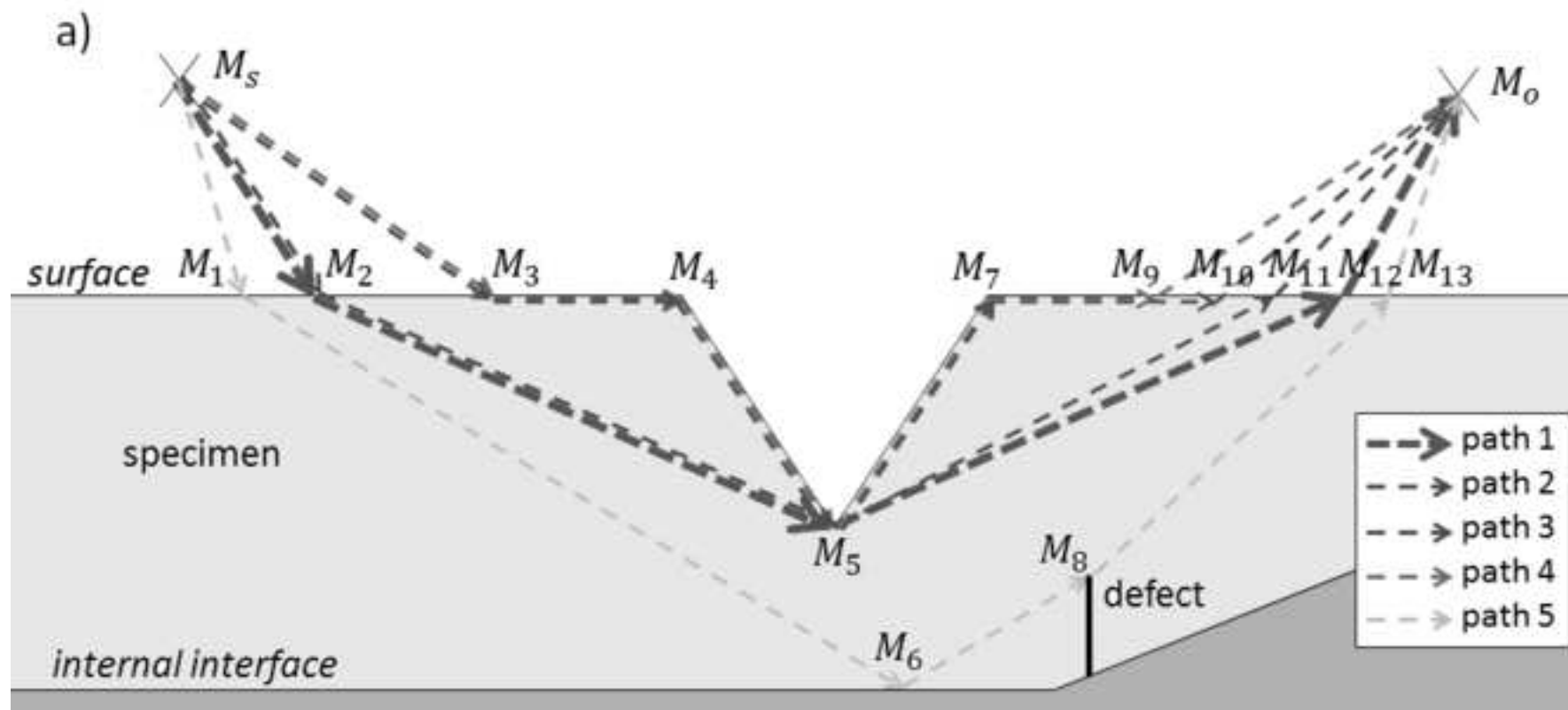


Figure 7

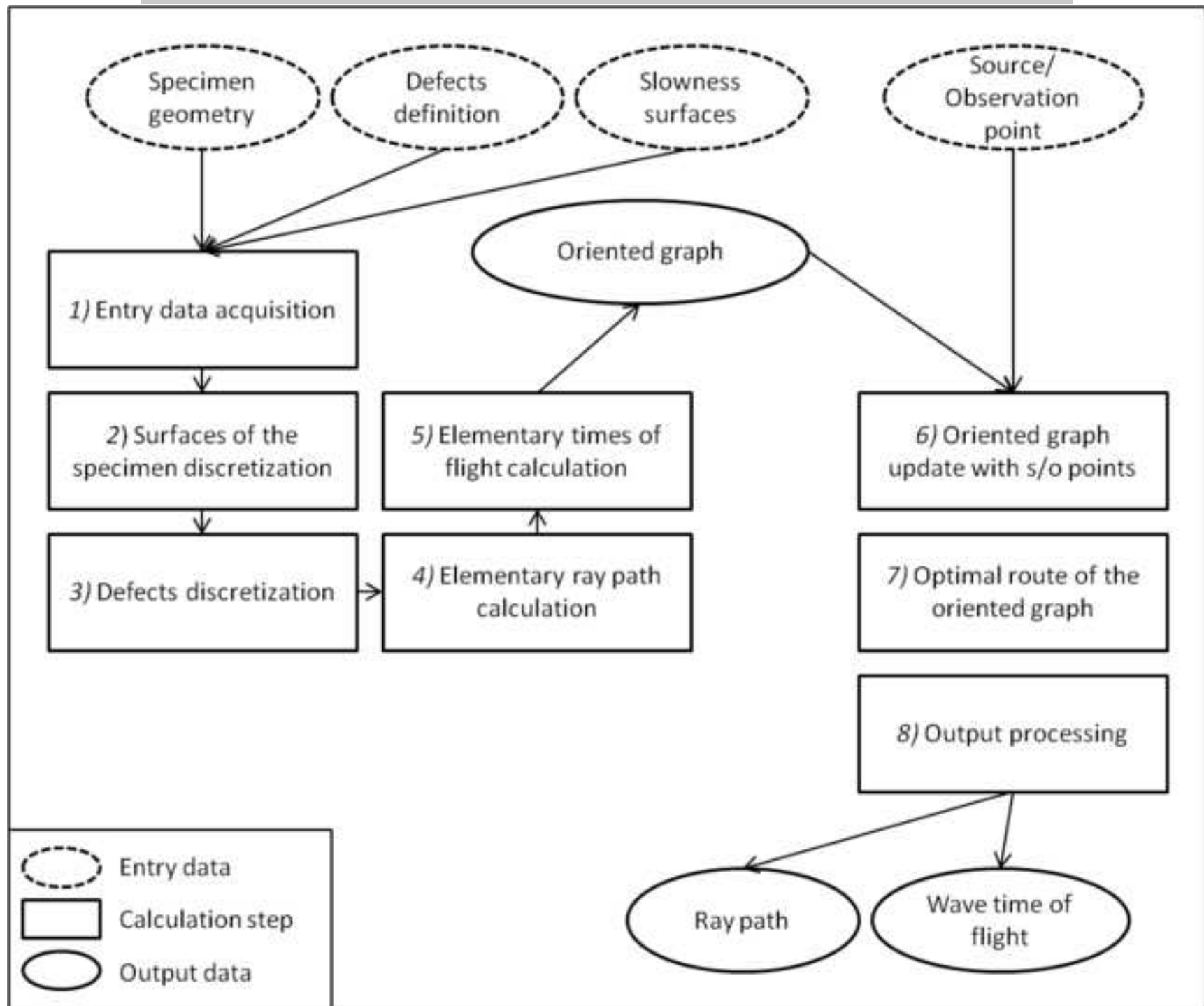
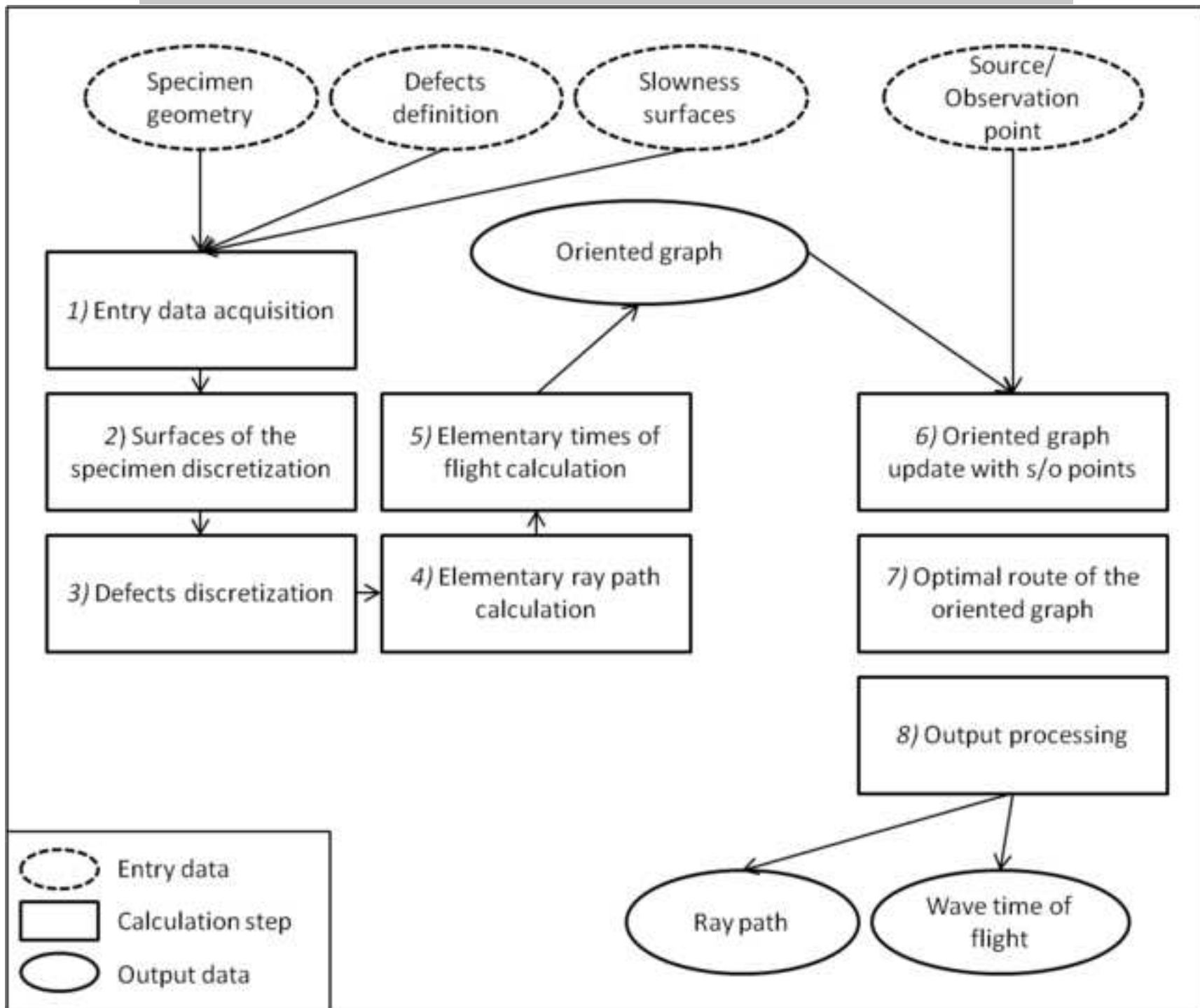
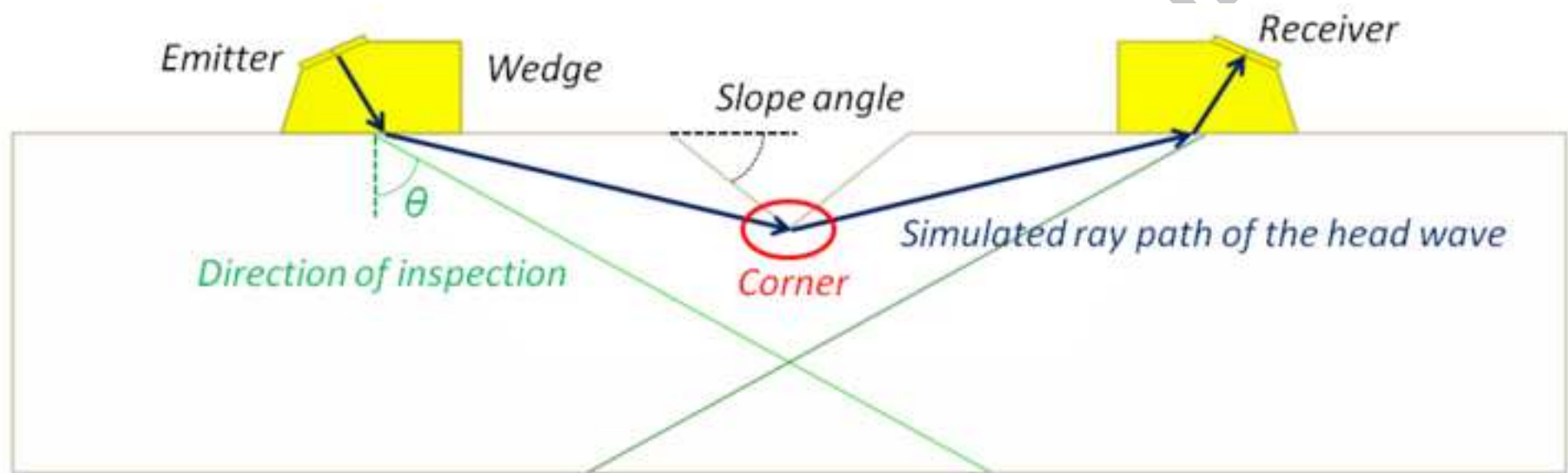
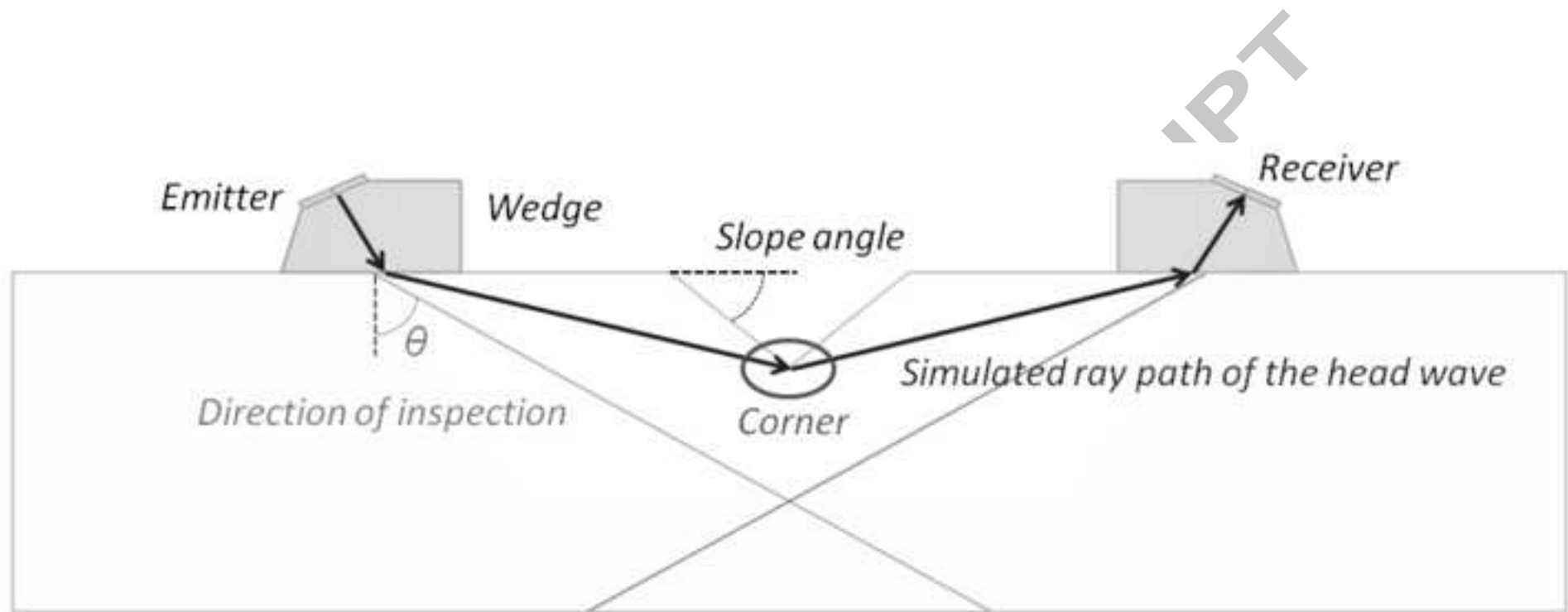
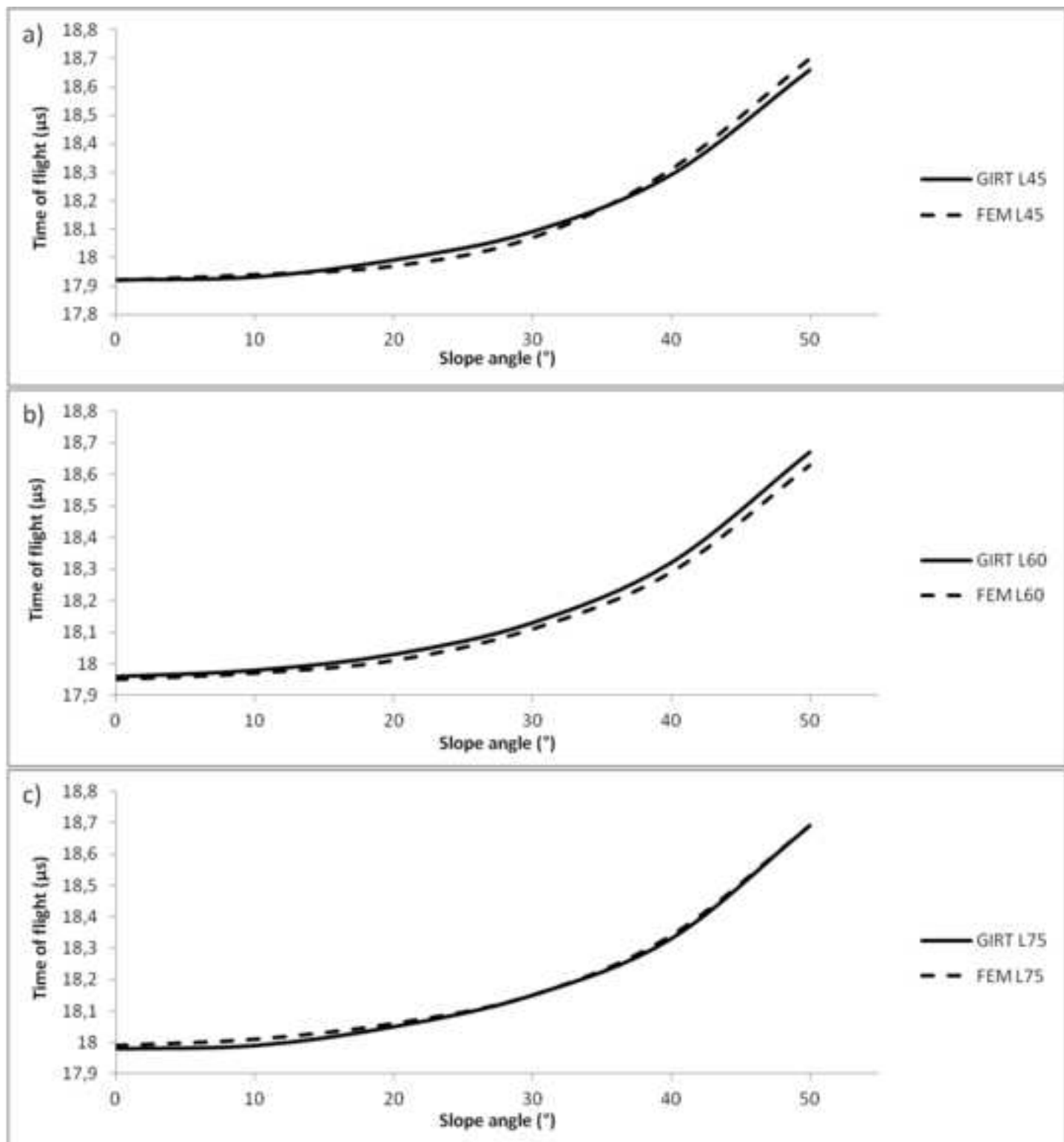


Figure 7 (b&amp;w)









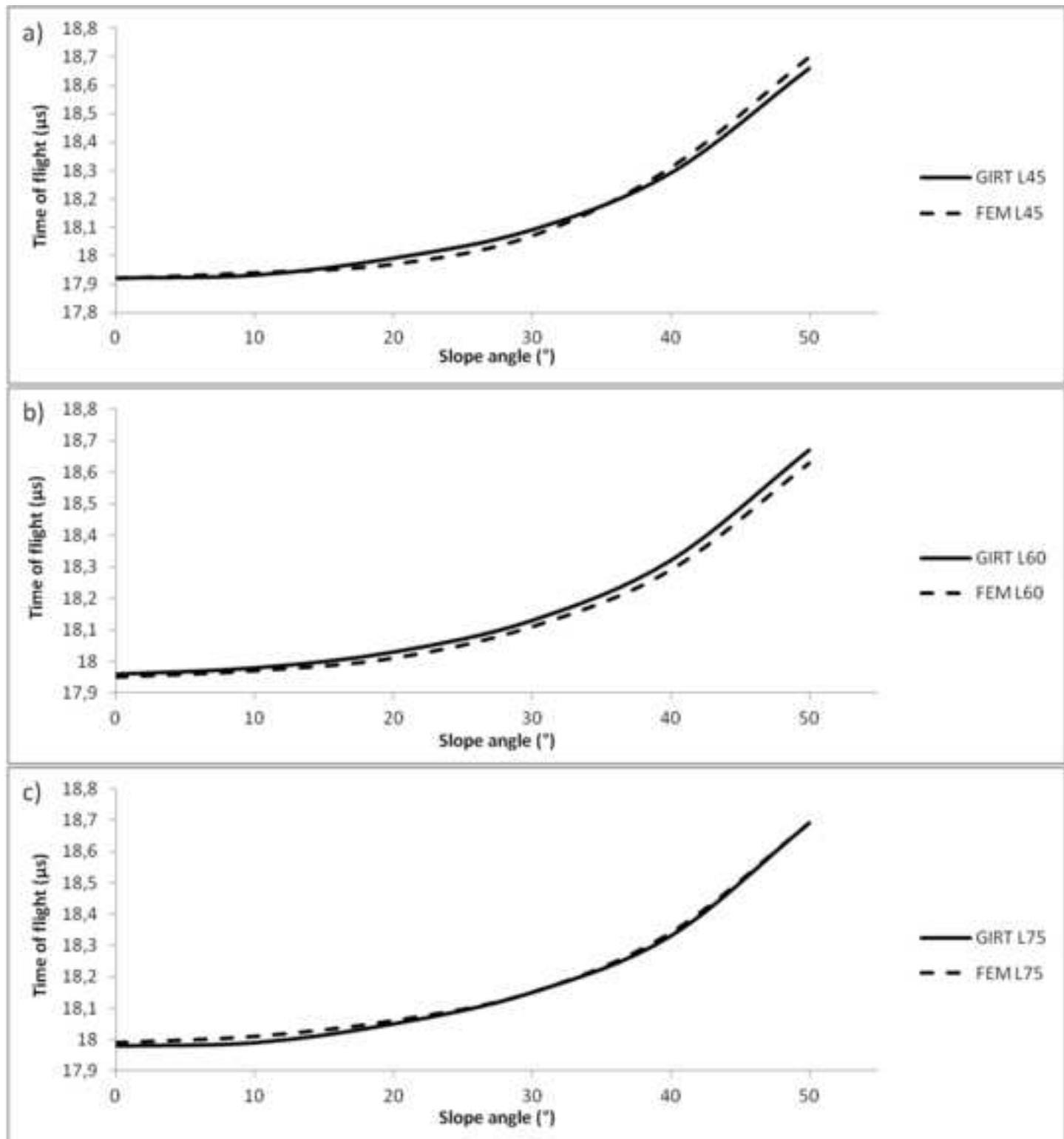


Figure 10 (revised)

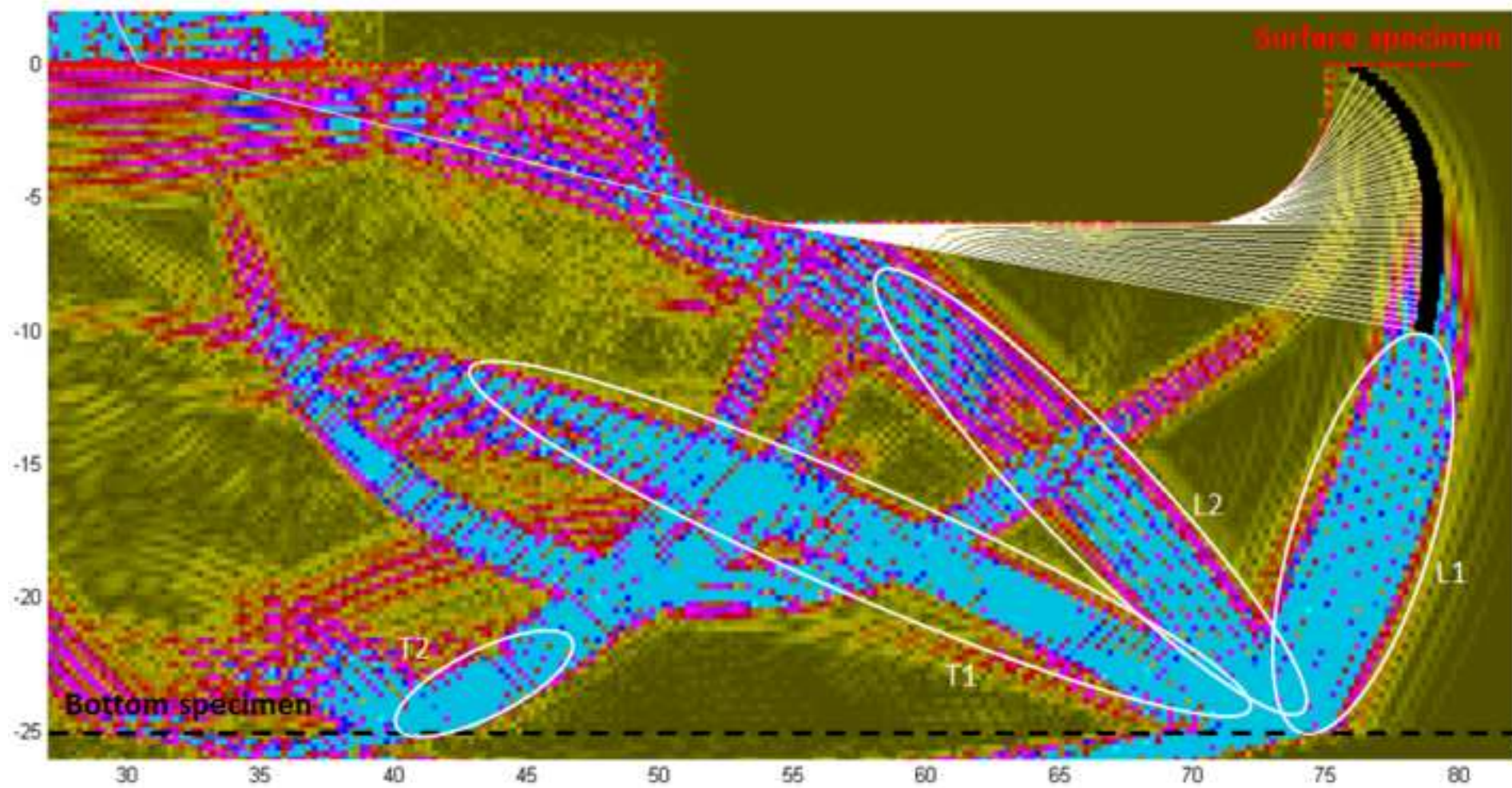
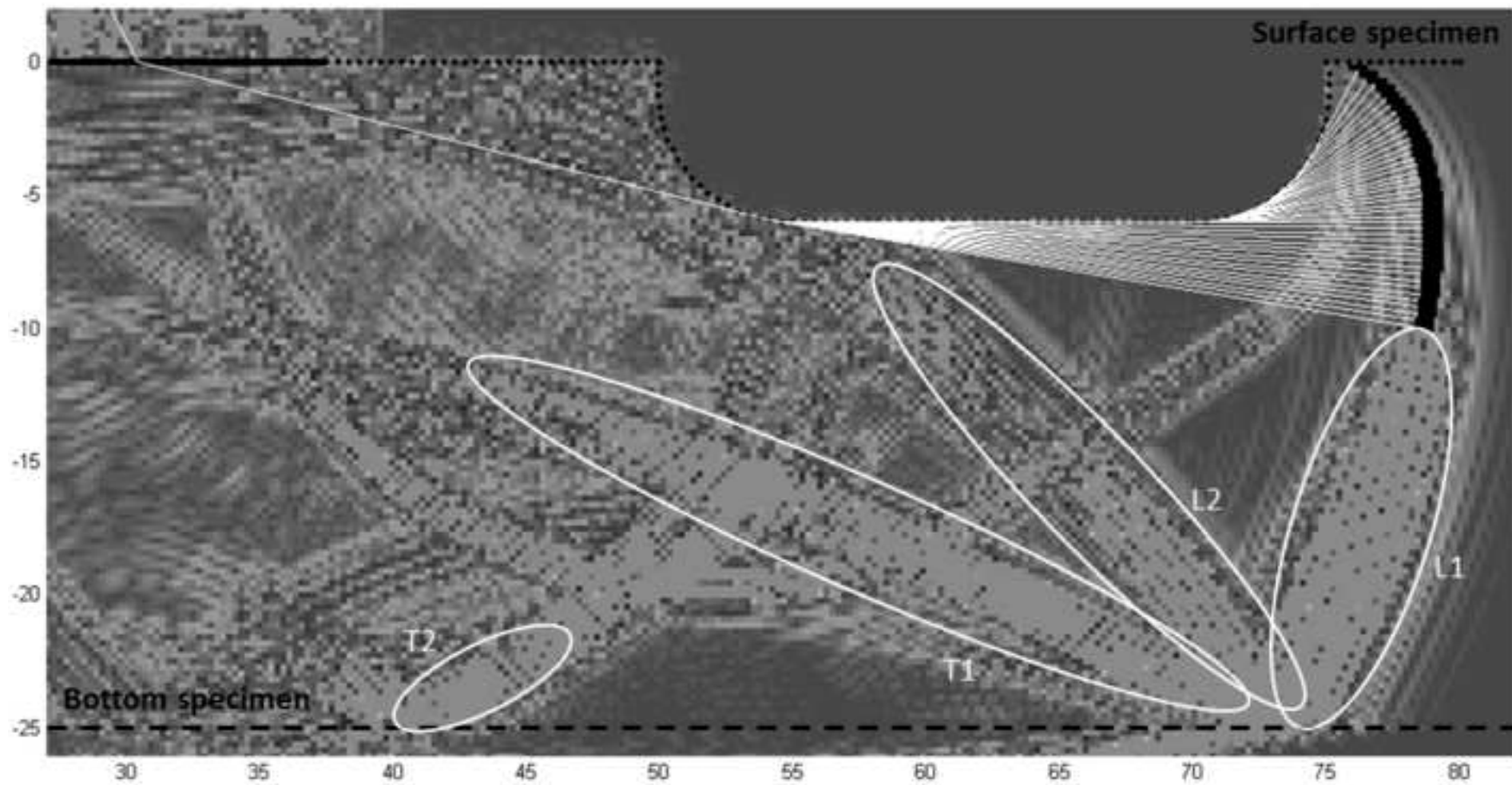
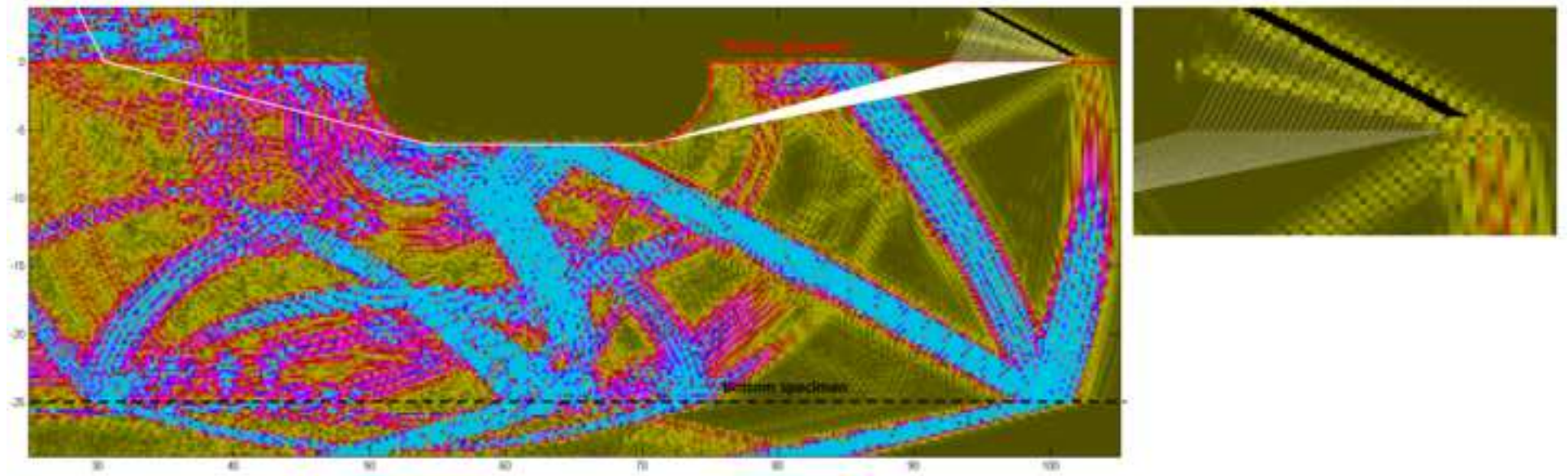
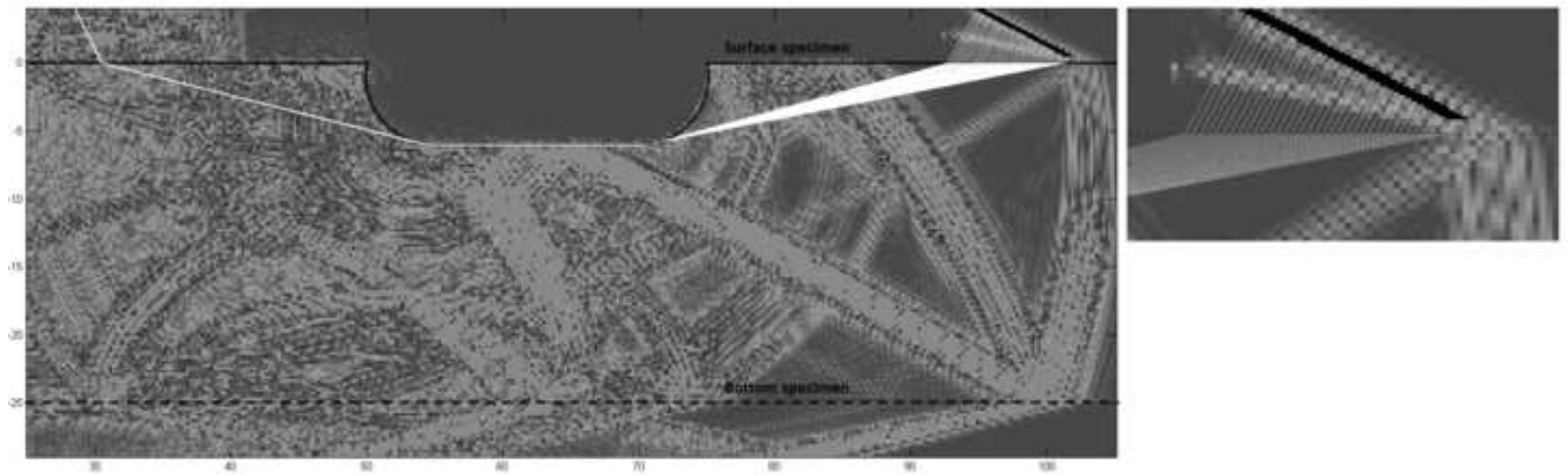
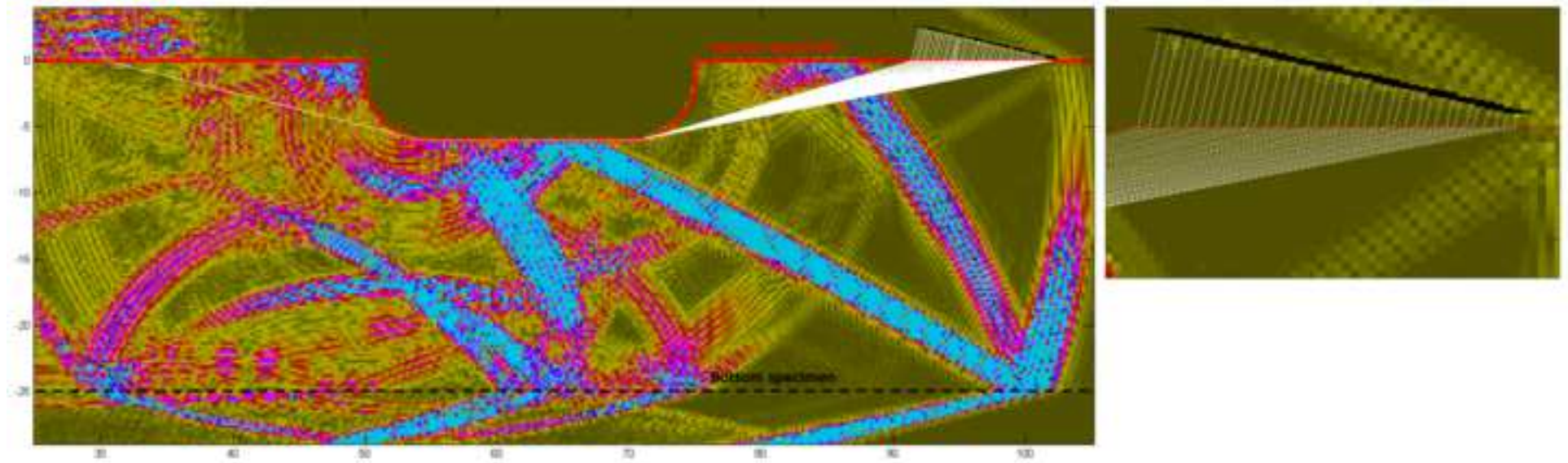


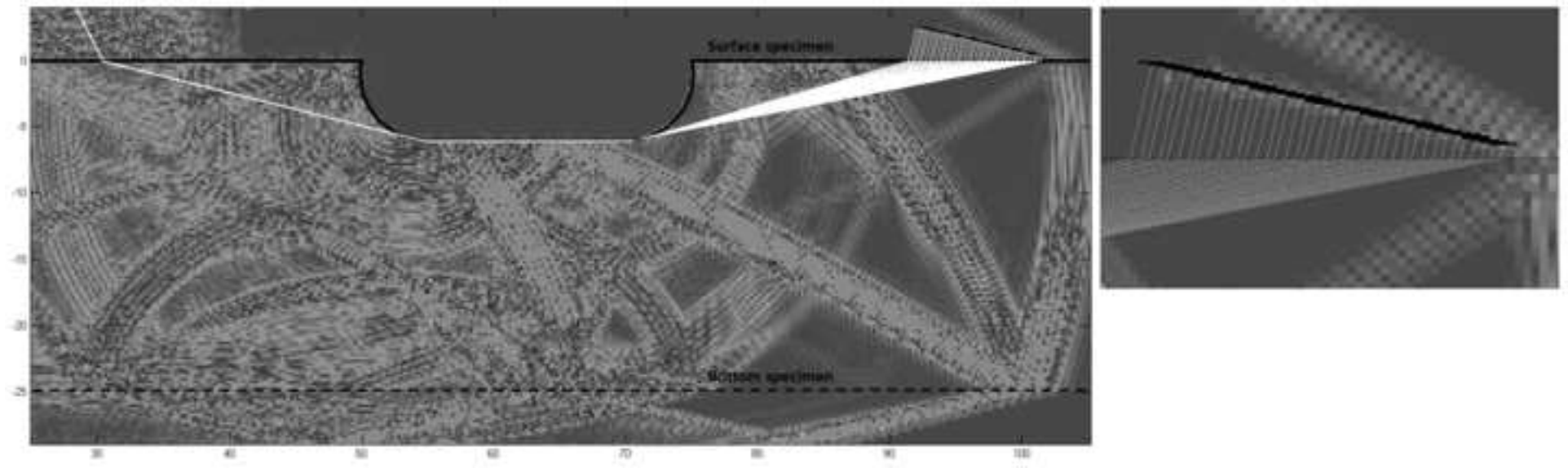
Figure 10 (b&w) (revised)

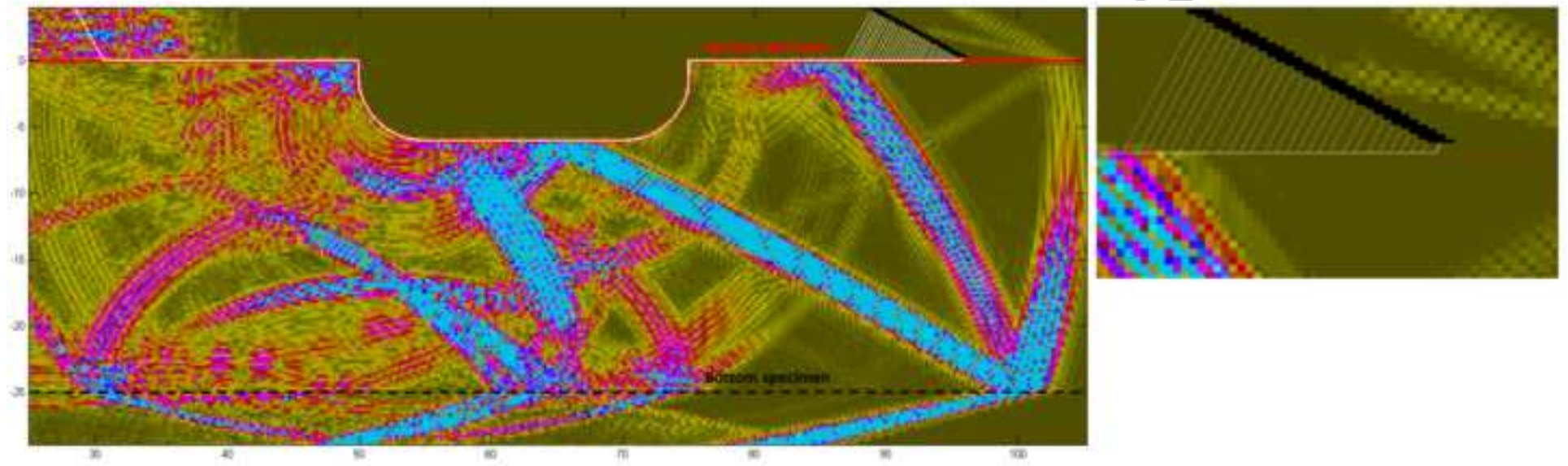


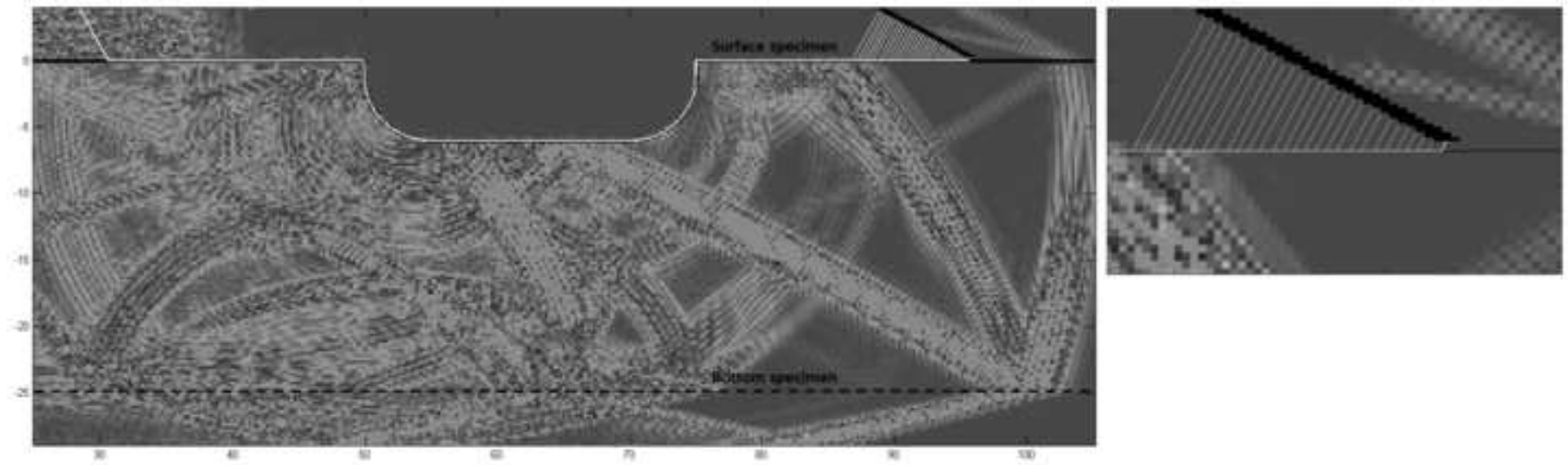












- This article provides a modeling study of head waves near irregular surfaces in NDT.
- Head wave propagation near such complex surfaces implies bulk mechanisms.
- A generic algorithm of ray tracing between interface points (GIRT) is developed.
- GIRT, based on Generalized Fermat's Principle, models effects of complex surfaces.
- The head wave fronts computed by GIRT are in good agreement with FEM simulations.

ACCEPTED MANUSCRIPT